Memoirs of the School of Engineering, Nagoya University
Vol.52, No.2 (2000)

STRENGTH ANOMALY OF β-CuZn

Hiroyasu SAKA

Department of Quantum Engineering
and Department of Materials Science and Engineering

(Receiveed February 7, 2001)

Abstract

Mechanical properties of single crystals of β-brass have been studied extensively as functions of deformation temperature and orientation. Yield stresses show anomalous peaks at around 200°C, the exact peak temperature (Tp) depending on both orientation and mode in which crystals are deformed., i.e. tension, compression or direct shear. Dislocation structures have been observed comprehensively using transmission electron microscopy. Below Tp , <111> dislocations are activated, while above Tp , non-<111> dislocations such as <100> and <110> dislocations are activated. In addition between room temperature and Tp, where the yield stress shows an inverse temperature dependence, <111> dislocations are climb-dissociated. The climb dissociation of <111> dislocations below Tp and transition of slip direction across Tp are attributed to the strength anomaly in β-brass. However, a β-brass single crystal with orientation $\chi = 30°$ shows very peculiar plasticity, which can not be explained easily at the moment.

1. Introduction

Generally most of solids soften at high temperatures. The yield stresses of these materials decrease monotonously with increasing deformation temperature. However, there are some exceptions. For example, in some kinds of long range ordered alloys and intermetallic compounds the yield stress increases with increasing temperature in a limited temperature range. Among those showing the strength anomaly, β-brass is of particular interest. The structure of β-brass is very simple; it crystallizes in B2 or CsCl type, as shown in fig. 1. The corner is occupied by one of the component atoms, say Cu and the centre is occupied by the other, say Zn. By contrast, the mechanical behaviour is puzzlingly complicated.

The present author has studied the strength anomaly of β-brass over the past two decades (Saka 1984; Saka and Kawase 1984; Saka *et al.* 1984; Saka and Zhu, 1985, 1989, 1994; Saka *et al.* 1985; Zhu and Saka, 1986, 1989). Although the mechanism of the strength anomaly is not understood completely, it would be worth summarizing the experimental results obtained so far to promote further study on this very familiar yet puzzling material.

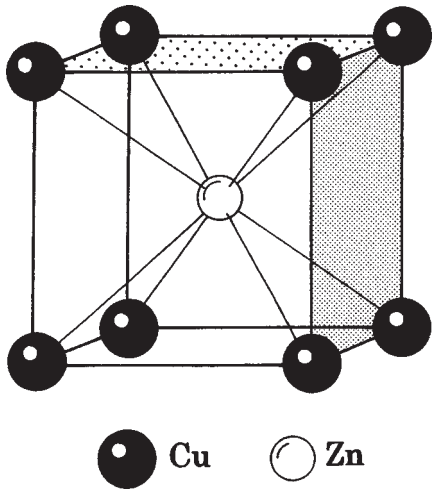

Fig. 1 Crystal structure of β-brass.

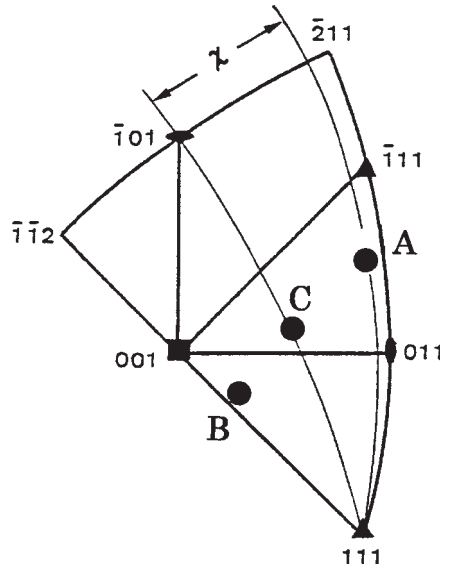

Fig. 2 Axial orientation of crystals used. The orientation parameter χ is defined as the angle between the normal of maximum resolved shear stress plane and the pole of the (101) slip plane when [111] is taken as the slip direction.

2. Growth of Single Crystals

Single crystals of β-brass were grown by the Bridgman technique in an argon atmosphere from Cu and Zn, both of four-nines purity, in the form of a rod 2.5 cm in diameter and 5 cm long. For both tensile and compression tests, rectangular specimens with a cross section of 3 mm $\times$ 3 mm were sectioned using a mulit-wire abrasive saw. They were annealed at 700°C for 30 min in an argon atmosphere and furnace-cooled. Figure 3 shows the axial orientations (A, B and C[*]) of crystals used for tension and compression tests.

Here, the orientation parameter χ is defined as the angle between the normal of the maximum resolved shear stress plane and the pole of the $(\bar{1}01)$ slip plane when [111] is taken as the slip direction. The specimens used for pure shear will be described in Sections 9 and 10 in detail.

3. Stress-Strain Curves

Figure 3 shows some typical examples of stress-strain curves, and fig. 4 shows the temperature dependence of the yield stress for single crystals with different orientations deformed in ten-

* Unfortunately, the notations for orientations A, B and C used in the previous papers (Saka and Kawase 1984; Saka *et al.*, 1984; Saka and Zhu,1985, 1989, 1994; Saka *et al.*, 1985; Zhu and Saka, 1986, 1989) were not identical.

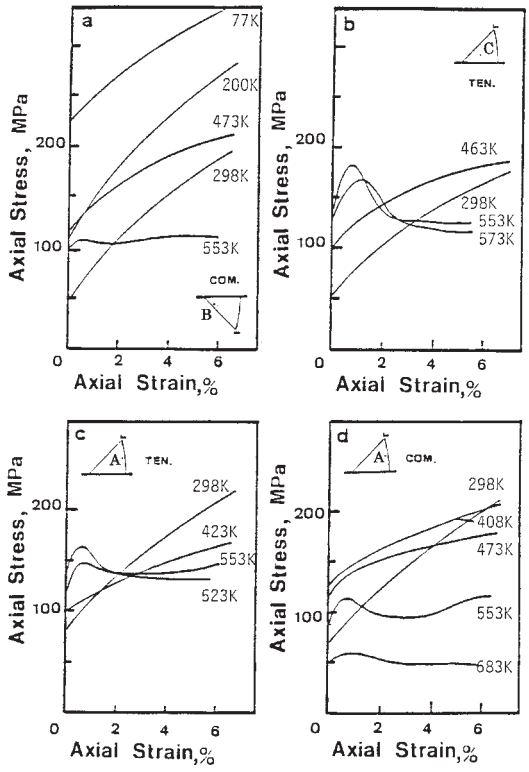

Fig. 3 A selection of axial stress-strain curves of crystals with the three different orientations deformed in tension or compression.

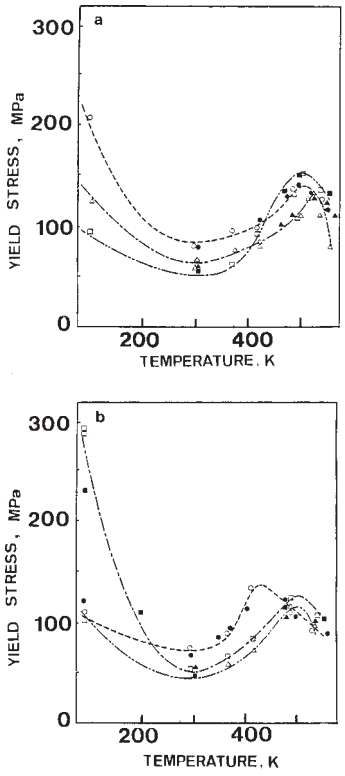

Fig. 4. Temperature dependence of the yield stress (a) in tension and (b) in compression in the three deformation orientations: ○, ●, orientation A; □, ■, orientation B; △, ▲, orientation C; □, △, ○, from Nohara *et al.* (1984); ■, ▲, ●, results obtained Saka and Zhu (1989).

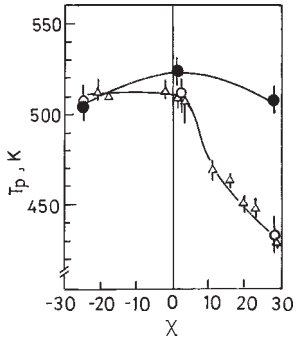

Fig. 5 Orientation dependence of Tp obtained in tensile tests (●) and in compressive tests (○, △); △, results obtained by Umakoshi *et al.* (1977).

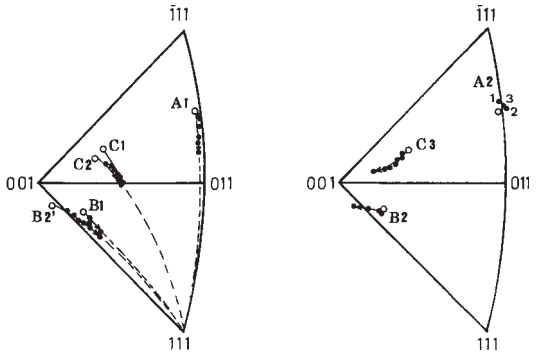

Fig. 6 Stereographic representations of specimen axes during tensile deformation of β-CuZn, The initial orientations are denoted by ○. (a) Below Tp; crystals A1, B1 and C2' were deformed at room temperature and crystals C1 at 200°C, (b) Above Tp; crystals A2, B2 and C3 were deformed at 280°C.

sion and compression. Above room temperature the yield stress increases and shows peaks at around 200°C for all the cases studied. However, the temperature at which the yield stress shows the peak (hereafter denoted by Tp) depends not only on the orientation but also on the mode in which the crystals were deformed. Figure 5 shows the orientation dependence of Tp when crystals are deformed in compression and in tension. The Tp value obtained in compression depends on χ asymmetrically in such a way that Tp is constant for $\chi < 0°$ and decreases for $\chi > 0°$. These results are in good agreement with those obtained by Umakoshi *et al.* (1977). In contrast, the Tp value obtained in tension depends on χ in a symmetrical manner.

4. Slip Systems and Dislocations Structure

4.1 Experimental procedures

Single crystals were deformed in tension and in compression at room temperature, 200 and 280°C. Slip planes were determined by analyzing the slip traces on the crystal surfaces (Nohara *et al.* 1984). The reorientations of single crystals during tensile tests were studied by the X-ray Laue method, and the macroscopic slip directions determined from analyses of the variation of the axial orientations. From the deformed crystals foil specimens were prepared by eletropolishing using D2 solution in a Tenupol automatic thinner. The specimens were examined in a Hitachi HU-1000D high-voltage electron microscope (operated at 1000 kV) or JOEL 200 CX and Hitachi H-800 microscopes (both operated at 200 kV). Dislocations were imaged using high-ordered reflection technique (Bell and Thomas 1972), in which the standard $\mathbf{g}.\mathbf{b} = 0$ invisibility criterion (Hirsch *et al.* 1965) can be applied, even for such an elastically anisotropic crystal as β-brass (Saka 1984).

4.2 Results

Figure 6 shows the reorientation of crystals A, B and C deformed in tension below and above Tp. Below Tp (fig.6(a)) the orientations varied towards [111] along the great circles connecting the initial tensile orientations and [111] for all the crystal studied (A1,B1,B2',C1 and C2). It should be pointed out that crystal B2' was deformed at room temperature (below Tp) after having been deformed at 280°C (above Tp) as was crystal B2. It is clear that the crystal slipped along [111] during the second deformation at room temperature. Thus, it can be said that the macroscopic slip direction of [111] observed below Tp does not depend on the initial conditions of the crystals. However, this point will be discussed in more detail in Sec. 5.

In contrast, above Tp (fig.6(b)) the orientations did not rotate towards [111]; the orientations of crystals C3 and B2 rotated towards [001] along the great circles connecting the initial orientations and [001], while that of crystal A2 remained virtually unchanged up to a strain 13%. In addition, the Laue spots from crystal A2 deformed above Tp became diffuse at a rather small strain.

Figure 7 shows a typical dislocation structure of crystal A deformed at room temperature, well below Tp. In fig.7(a) the dislocations were imaged in $\mathbf{g} = 020$, and most of the dislocations showed strong contrast. The dislocations in fig.7(b), however, were imaged in $\mathbf{g} = 1\bar{2}1$ and most of them were faint. This contrast experiment indicates that the Burgers vector of these dislocations is parallel to [111]. High-resolution weak-beam micrographs of these dislocations showed that they consist of two superpartials with Burgers vector 1/2[111] (Saka 1984). Essentially similar features were observed in dislocations structures of those crystals which were deformed below Tp despite of whether they were deformed in tension or compression.

The dislocation structure of crystals deformed at around Tp was quite different from that of crystals deformed below Tp. Figure 8 shows a typical dislocation structure of crystal A, deformed

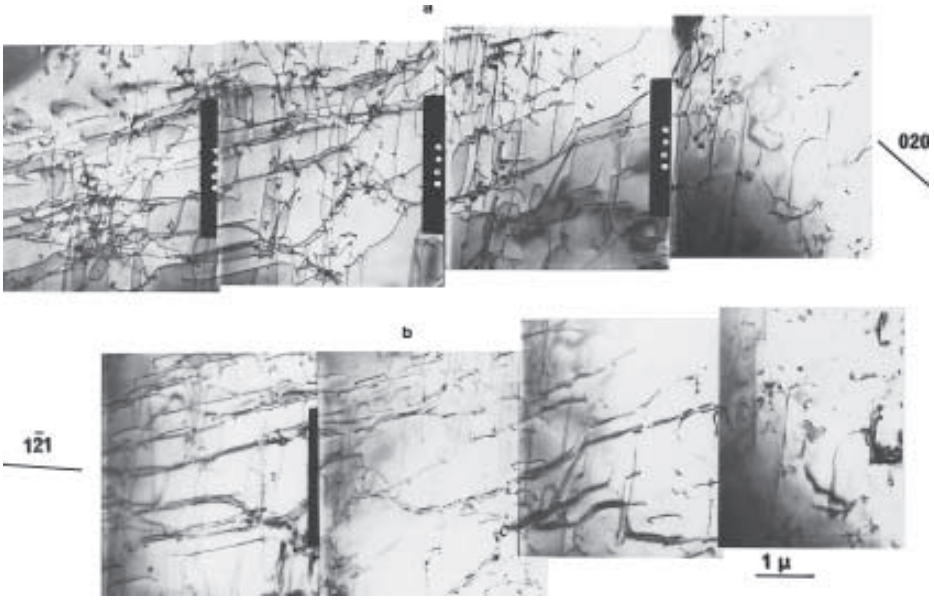

Fig. 7 Dislocation configuration in crystal A deformed at room temperature and imaged in (a) **g** = 020 and (b) **g** = 121. Most of the dislocations disappear in (b), indicating that the Burgers vector of these dislocations is parallel to [111].

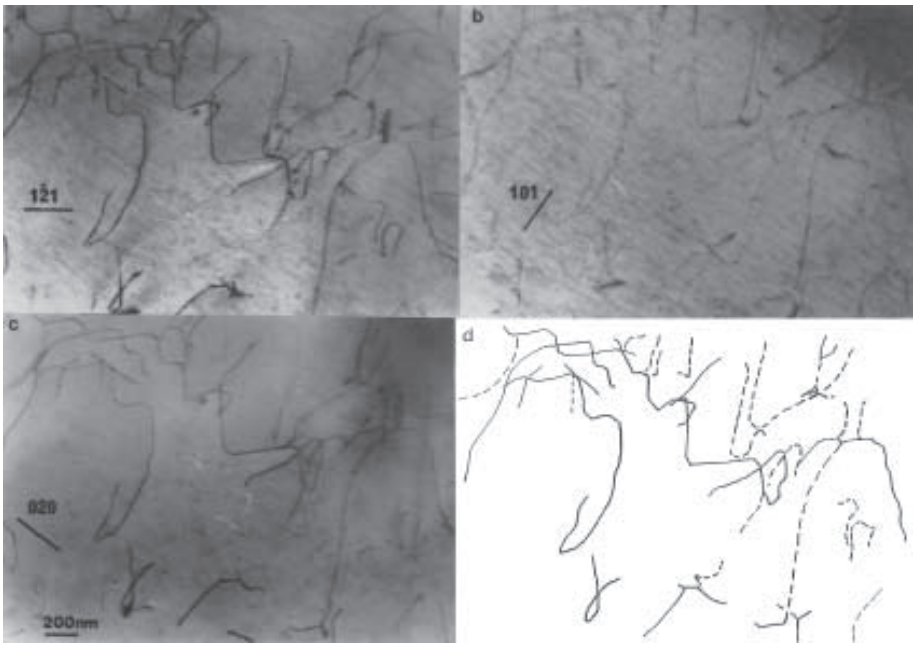

Fig. 8 Dislocation configuration in crystal A deformed at 200°C (above Tp). The dislocations are imaged in (a) **g** = 1$\bar{2}$1, (b) **g** = 101 and (c) **g** = 020. Most of the dislocations disappear either in **g** = 101 or **g** = 020, indicating that the Burgers vectors are [010] and [101], respectively. (d) A schematic sketch of the [010] and [101] dislocations.

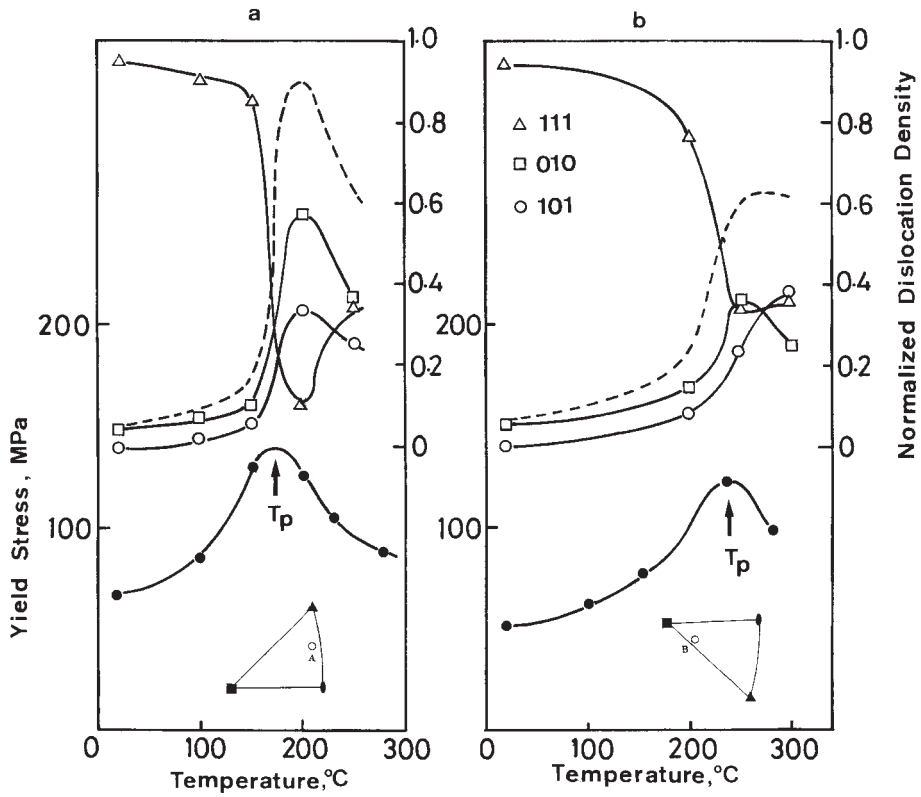

Fig. 9 Normalized densities of [111], [010] and [101] dislocations plotted against the deformation temperature, together with the axial yield stress (●) for crystals A(a) and B(b). The dashed lines indicate the densities of non-[111] dislocations, i.e. the sum of [010] and [101] dislocations.

in compression at 200°C (above Tp), imaged in $\mathbf{g} = 1\bar{2}1$, 101 and 020. Most of the dislocations disappear in either $\mathbf{g} = 101$ or $\mathbf{g} = 020$, indicating that the Burgers vectors of these dislocations are [010] and [101], respectively. Figure 8(d) shows a schematic sketch of those [010] and [101] dislocations. It can be seen from fig.8 that the [010] and [101] dislocations form complex dislocation networks in the plane of foil, which is parallel to $(\bar{1}01)$. Thus, the slip plane of these dislocations is identified as the $(\bar{1}01)$ plane.

The density of [111], [101] and [010] dislocations were measured as a function of the deformation temperature for crystals A and B. Only those dislocations that lie in the plane of foil, i.e., $(\bar{1}01)$, were studied, and the normalized densities of [111], [101] and [010] dislocations were obtained by dividing the length of the respective dislocations by the total length of dislocations studied. Thus, in this measurement an error arising from an uncertainty in estimating the thickness of specimens, which is considered to be the main source of error in estimating the dislocation density from electron micrographs, is eliminated.

The results are shown in fig.9. It is clear that below Tp most of the dislocations are [111] superlattice dislocations consisting of two superpartials, while around Tp the density of [111] dislocations decreased markedly; above Tp it appears that the density of [111] dislocations recovers, but it is still much lower than that of [101] or [010] dislocations. Figure 10 shows the dislocation structures as a function of the orientation and the deformation temperature, together with Tp for

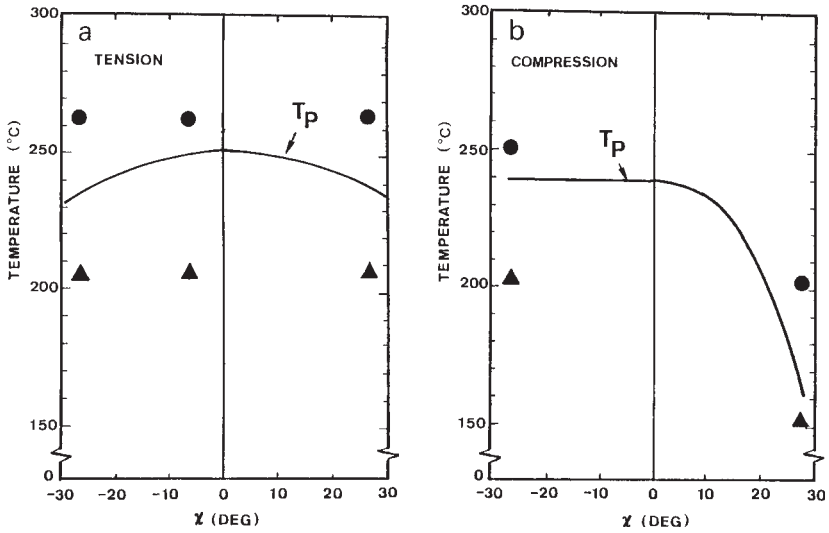

Fig. 10 The orientation and temperature dependence of dislocation structure of β-brass deformed in (a) tension and (b) compression (Saka and Kawase 1984). ▲ indicates dislocation structures where <111> dislocations are predominant, while ● indicates those where non-<111> dislocations are predominant.

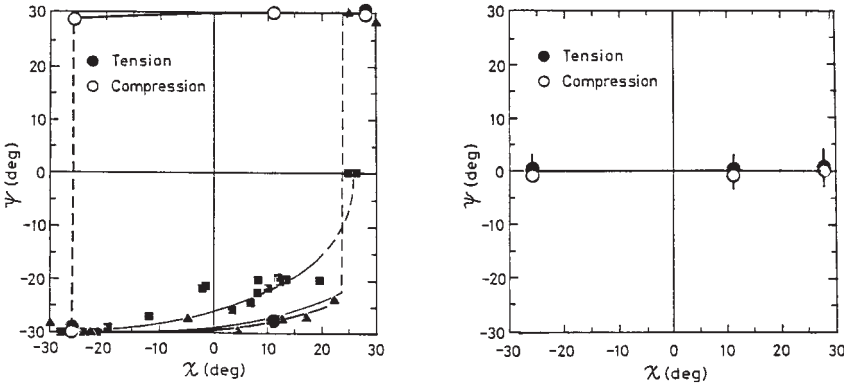

Fig. 11 $\psi - \chi$ curves for tension (full symbols) and compression (open symbols) at 77K(a) and room temperature (b). Circles (both open and full) by Nohara *et al.* (1984); ■ tension by Hanada and Izumi (1977), ▲ by Tekeuchi *et al.* (1982).

both tension and compression. It can be seen that there is an excellent correspondence between the transition of dislocation structure (from <111> type to non-<111> type) and the occurrence of the stress peak, for crystals deformed in both tension and compression.

Figure 11 shows orientation dependence of the operative slip planes at 77K (Nohara *et al.* 1984). At 77K the $\psi - \chi$ curves in tension and compression are approximately symmetric with each other with respect to the origin, where ψ is the angle between the observed slip plane and the reference $(\bar{1}01)$ plane. On the other hand, above Tp the concept of the $\psi - \chi$ curve itself is of no meaning, since the slip direction is no longer along <111>.

5. Effect of Pre-straining

5.1 Experimental procedures

Specimens with orientations A and B were pre-strained in either tension or compression mostly at room temperature except a few cases and then deformed between 100 and 250°C again in either tension or compression. Thus, crystals were deformed in four different combinations of the pre-straining and the second run of deformation (table 1*). Crystals of the series CC were pre-strained in compression at room temperature and then deformed in compression in the second run of deformation. Crystals of the series CT were pre-strained in compression at room temperature and deformed in tension in the second run of deformation. Similar nomenclatures are applied to the series of TT and TC. The re-orientations of single crystals CT(A) and TT(A) during the second run of deformation in tension at 200°C were studied by the X-ray Laue method, and the macroscopic slip directions determined from the analyses of the variation in tensile orientations.

5.2 Results

5.2.1 Yield stress

Figure 12(a) shows the yield stress of the pre-strained (at room temperature) crystals with the initial orientation A as a function of temperature where the second deformation was carried out, together with the yield stress of virgin crystals deformed in compression and in tension (Nohara *et al.* 1984). Apart from a slightly higher stress level of the pre-strained crystals, which can be attributed presumably to an increase in the internal stress level due to the work hardening during pre-straining at room temperature, it is clear that Tp for those crystals pre-strained in compression at room temperature (CC(A) and CT(A)) coincides with that of virgin crystals deformed in compression and that Tp for those pre-strained in tension at room temperature (TC(A) and TT(A)) coincides with Tp for a virgin crystal deformed in tension. Figure 12(b) shows the yield stress of pre-strained crystals with the initial orientation of B as a function of the temperature of the second deformation. It is clear that the value of Tp of crystals with the initial orientation A pre-strained in tension is close to that of crystals with the initial orientation B pre-strained in compression and vice versa.

Table 1 Specimens used in prestraining tests

Crystal Number	Prestraining		Second Deformation at high temperatures
	Temperature	Mode of prestraining	Mode
TC(A)	RT	Tension	Compression
CC(A)	RT	Compression	Tension
CT(A)	RT	Compression	Tension
TT(A)	RT	Tension	Tension
CC'(A)	77K	Compression	Compression
CC"(A)	373K	Compression	Compression
TC(B)	RT	Tension	Compression
CC(B)	RT	Compression	Compression

* The orientation of a crystal is denoted by A or B in the parenthesis like CT(A). That is, a crystal with orientation A was deformed in compression in the first deformation, followed by deformation in tension in the second run.

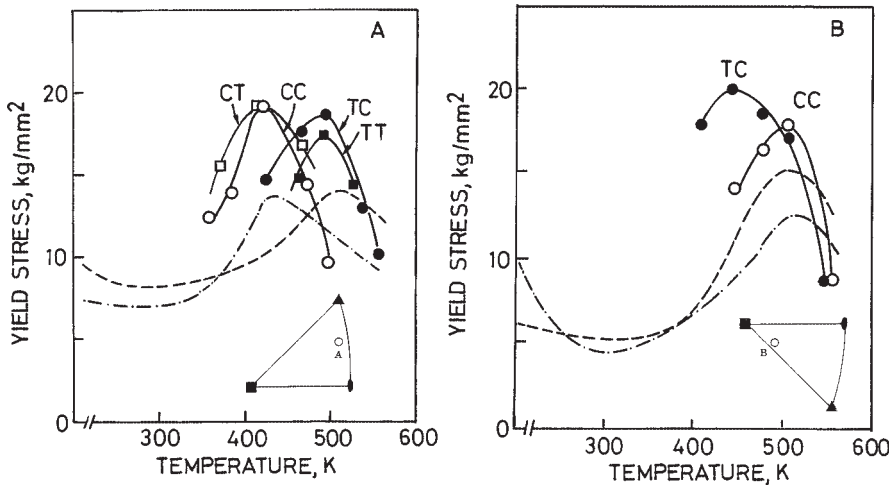

Fig. 12 Yield stresses of β-brass single crystals with orientations A(a) and B(b) pre-strained at room temperature as a function of the temperature at which the second deformation is carried out. Data for the yield stress obtained on virgin crystals deformed in compression (-•-) and in tension (---) are also shown (Nohara *et al.* 1984).

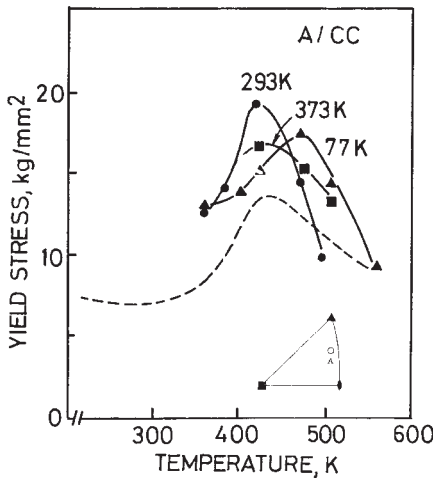

Fig. 13 Temperature dependence of the yield stress of β-brass single crystals with orientation A, which are pre-strained in compression and then deformed in compression in the second test (CC(A)). Data for the yield stress obtained on virgin crystals deformed in compression (-•-) are also shown (Nohara *et al.* 1984).

Figure 13 shows the yield stress of crystal with the initial orientation A pre-strained in compression at 77(CC'(A)) and 373K(CC"(A)), together with data for virgin crystals. It is clear that the value of Tp of crystals pre-strained at room temperature and 373K is lower than that of those pre-strained at 77K.

5.2.2 Reorientation of pre-strained crystals during deformation at 200°C

Figure 14 shows the reorientation of crystals TT(A) and CT(A) during pre-straining at room temperature and also during the second run of deformation at 200°C. During pre-straining of crys-

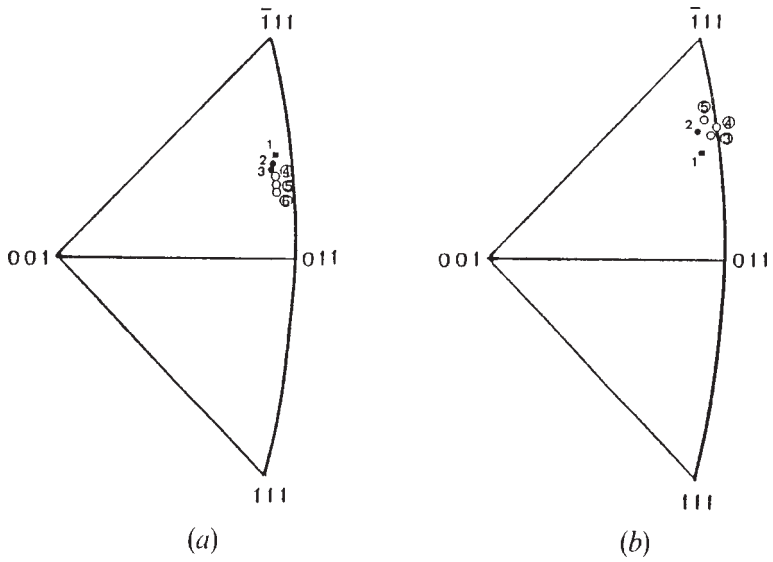

Fig. 14 Stereographic representations of specimen axes of (a) TT'(A) and (b) CT'(A). The initial orientations (before pre-straining at room temperature) are denoted by full squares (■), and reorientations during room-temperature pre-straining are indicated by full circles(●); the numerals attached to each of the data points refer to the chronological order.

tal TT(A) at room temperature, the reorientation varied away from [111] along the great circle connecting the initial orientation and [111], indicating that slip took place along [111]; this is in good agreement with the previous results. The behaviour of reorientation of TT(A) during the second deformation at 200°C is also similar to that of virgin crystal during room-temperature deformation.

In contrast, the behaviour of reorientation of crystal CT(A) during deformation at 200°C was quite different from that of TT(A). For crystal CT(A), the reorientation remained virtually unchanged up to a strain of 13%. This behaviour of reorientation is quite similar to that of virgin crystal deformed above Tp (Saka *et al.* 1985), indicating that the crystal CT(A) did not slip along [111] in the second deformation at 200°C, i.e. non-<111> slip took place.

Dislocation structures were examined by transmission electron microscopy and the Burgers vectors determined. The results indicate that, irrespective of the mode of the pre-straining at room temperature, below Tp in the second run of deformation <111> dislocations are predominating, while at and above Tp non-<111> dislocations are predominating. Thus, the results of the reorientation during the second run of deformation at 200°C are in excellent agreement with the results of transmission electron microscopy and the measurement of the yield stress.

6. Thin Specimens

6.1 Introduction

The contributions of edge and screw dislocations to the strength anomaly have been distinguished between by measuring the temperature dependence of the yield stresses of two types of

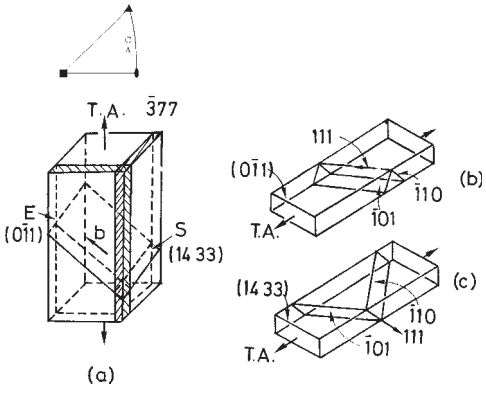

Fig. 15 The shape and orientation of thin crystals used. (a) Both S-type and E-type crystals have a common tensile axis (TA), namely $\bar{3}77$, but (b) in E-type crystals the primary [111] slip direction is contained in the plane defined by the width and tensile axis (side face), while (c) in S-type crystals, the primary slip vector is contained in the plane defined by the thickness and the tensile axes (top face).

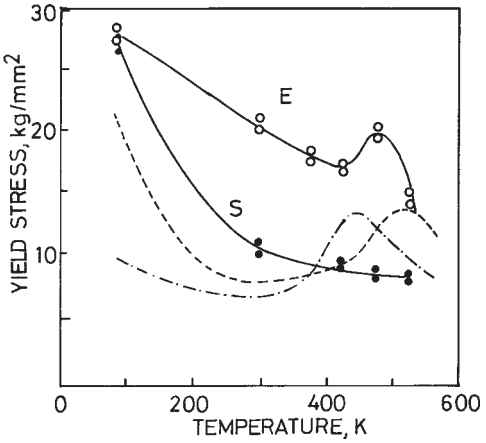

Fig. 16 Temperature dependence of yield stress of E-type (○) and S-type (●) thin crystals with orientation A. Data for the yield stress obtained on bulk crystals with orientation A deformed in tension (---) and compression (-•-) are also shown (Nohara *et al.* 1984).

thin crystal in which the deformation is carried mainly by edge dislocations or screw dislocations respectively.

6.2 Experimental Procedures

Two types of thin crystals, 100 μm in thickness, were cut with a multiwire saw from a bulk single crystal with the initial orientation A. Both of them had a common tensile orientation, namely $[\bar{3}77]$, but their surface normal orientation is either [14 3 3] or $[0\bar{1}1]$, as is shown in fig. 15(a). The geometry of slip systems in these thin crystals is illustrated in figs.15(b) and (c). In the crystal with (14 3 3) surface (hereafter denoted as the S-type crystal) the deformation is carried mostly by screw dislocations, while in the crystals with $(0\bar{1}1)$ surface (hereafter denoted as the E-type crystal) the deformation is carried mostly by edge dislocations. They were both deformed in tension at a strain rate of $2.0 \times 10^{-4}s^{-1}$ using an Instron-type tensile-testing machine. Grips, which had complete rotational freedom, were used in order to reduce the bending moment. The tests were carried out in the temperature range between 77 and 553K.

6.3 Results

Figure 16 shows the yield stress of thin crystals deformed in tension as a function of temperature, together with the yield stress of bulk virgin crystals deformed in tension as well as compression. The following features are evident.

(1) At a very low temperature, namely at 77K, both the S-type and the E-type crystals have high yield stresses, the differences of the yield stress between them being very small.

(2) Below room temperature the yield stress decreases with increasing temperature in the usual manner, but the yield stress of the S-type crystal decreases much more rapidly than that of the

E-type crystal.

(3) Above room temperature, the yield stress of the E-type crystal is nearly twice that of the S-type crystal. In addition, the yield stress against temperature curve of the S-type crystal is rather flat, while that of the E-type crystal shows a peak at around 473K.

(4) At room temperature the yield stress of thin crystals of both E and S type is higher than that of bulk crystals. Above room temperature, the yield stress of the E-type crystal is higher than that of bulk crystals, but the reverse is true for the S-type crystal.

7. Climb Dissociation-Core Structure of Dislocations

7.1 Introduction

In the foregoing sections, it has been shown that the transition of the slip direction in β-brass takes place at around 200°C, from <111> type at lower temperature to non-<111> type at higher temperatures. This transition is closely related to the occurrence of the anomalous peak in the curve of yield stress versus temperature in this material. However, the core structures of the <111> and non-<111> dislocations, which must control their activity, are not well understood. In this section, the core structures of <111> superdislocations as well as non-<111> dislocations were studied by weak-beam electron microscopy (Cockayne, Ray and Whelan 1969) to gain insight into the mechanism of the transition of the slip direction.

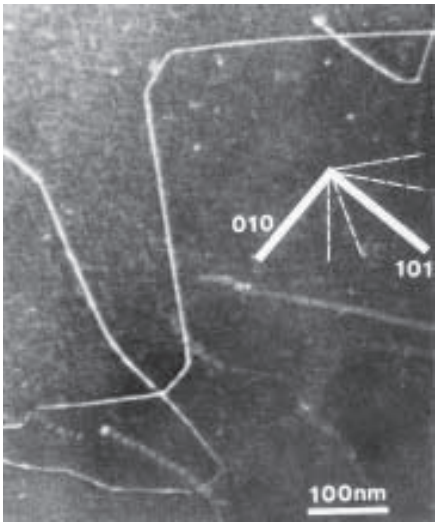

Fig. 17 Weak-beam micrograph of [010] dislocations. There is no evidence for their dissociation into two superpartials. In addition, they are bent sharply, indicating that the [010] dislocations have a strong directional instability; the hatched regions are those over which the [010] dislocations are stable (Head 1967).

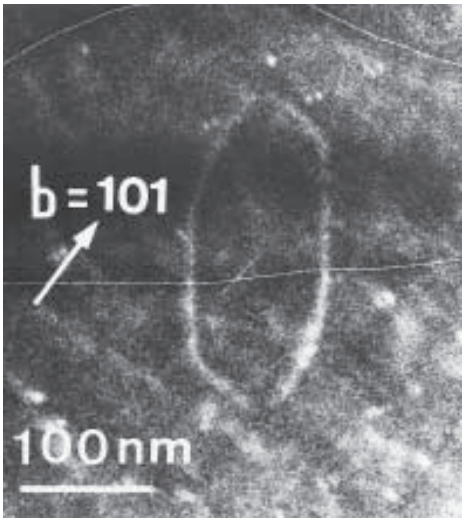

Fig. 18 Weak-beam micrograph of [101] dislocation loop. There is no evidence for their dissociation. The hexagonal shape indicates that the [101] dislocations have a directional instability. (The filamentary white lines running across the micrograph are cracks in the emulsion.)

7.2 Non-<111> dislocations

Figure 17 shows a weak-beam micrograph of [010] dislocations. They are bent sharply, indicating that the [010] dislocations have a strong directional instability; the hatched regions are those over which the [010] dislocations are stable (Head 1967). Figure 18 shows a weak-beam micrograph of a [101] dislocation. Again, the hexagonal shape indicates that the [101] dislocations have a directional instability. In neither case was evidence obtained for their consisting of more than one dislocation. This is in good agreement with a theoretical prediction that <010> and <101> dislocations are superdislocations which do not produce APB faults.

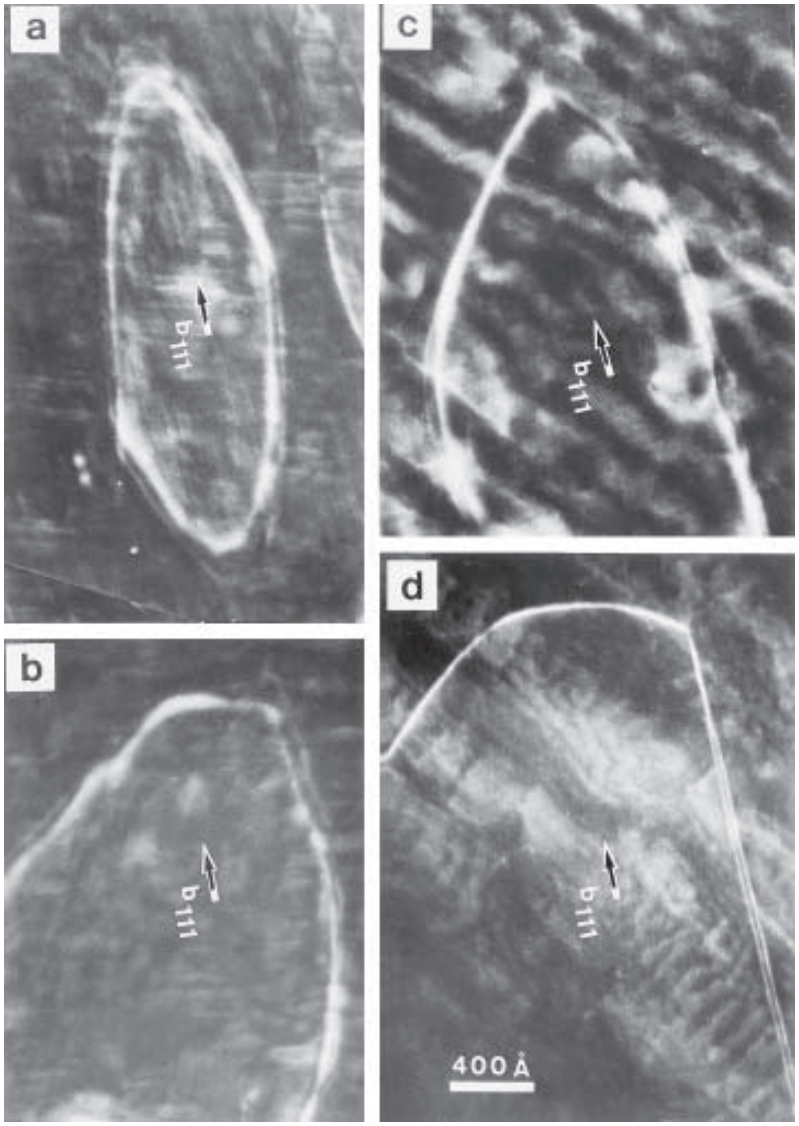

Fig. 19 Weak-beam electron micrographs showing the core structure of [111] superlattice dislocations in β-brass deformed at (a) 77K, (b) 200K, (c) 293K and (d) 463K (just below Tp).

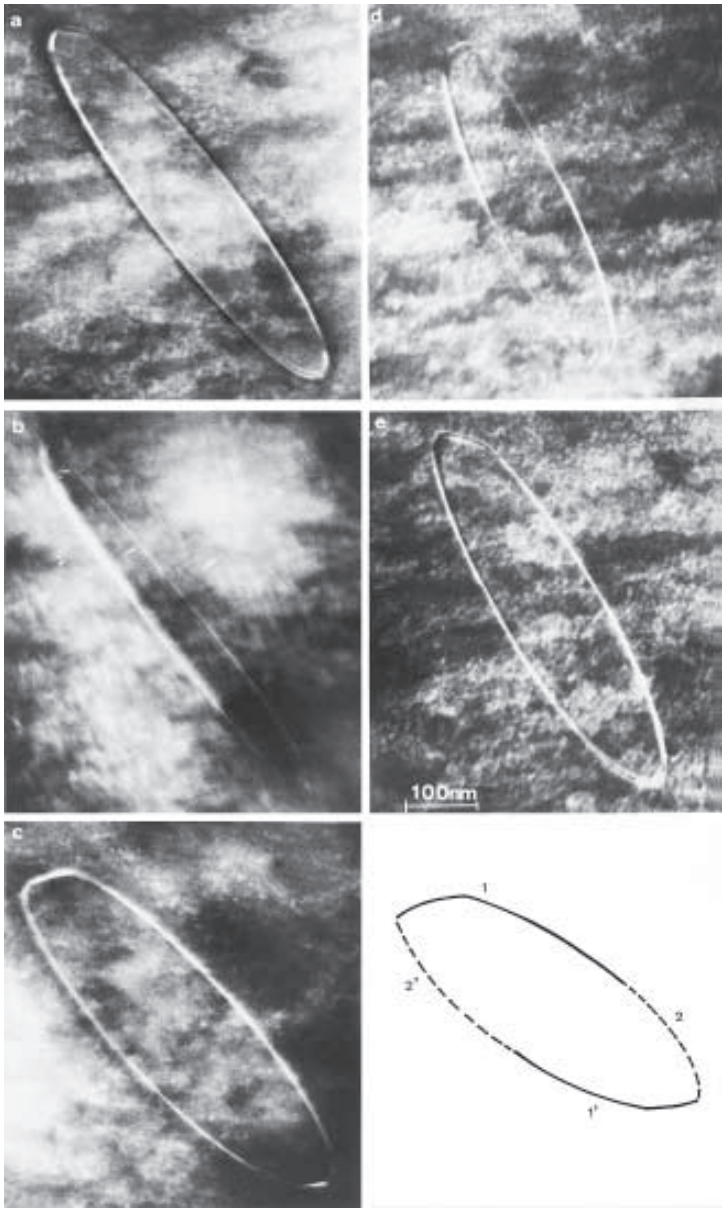

Fig. 20 A typical dislocation loop in a β-brass specimen which has been deformed at 463K and tilted by ± 30° around $1\bar{2}1$ and 121: (a) $\mathbf{g} = 1\bar{2}\bar{1}$, $\mathbf{B}\|\bar{1}01$; (b)$\mathbf{g} = \bar{1}\bar{2}\bar{1}$, $\mathbf{B}\|\bar{3}11$; (c)$\mathbf{g} = \bar{1}\bar{2}\bar{1}$, $\mathbf{B}\|\bar{1}\bar{1}3$; (d)$\mathbf{g} = \bar{1}\bar{1}0$, $\mathbf{B}\|\bar{1}13$; (e) $\mathbf{g}=0\bar{1}\bar{1}$, $\mathbf{B}\|\bar{3}\bar{1}1$; (f) sketch of the dislocation studied.

7.3 <111> dislocations

Figures 19(a)-(d) show typical examples of the weak-beam micrographs of dislocations introduced by deformations at 77, 200, 300 and 463K (all below Tp) respectively. At 77K, two superpartials of a <111> dislocation, in both edge and screw orientations, are resolved clearly, while at 463K, the two superpartials are not resolved or else their separation is very narrow. The situation for room temperature or 200K deformation lies just in between these two extremes. That is, at room temperature, the two superpartials in edge orientation are not resolved, while at least some in screw orientation are resolved clearly. At 200K the two superpartials are resolved along almost the whole length of the dislocation but, surprisingly, at some portions in edge orientation they are not resolved.

Figure 20 shows typical weak-beam micrographs of a [111] superdislocation in β-brass deformed at 190°C (above Tp). The Burgers vector of the dislocation was determined by a contrast experiment, using the high-order reflection imaging technique (Bell and Thomas 1972, Saka 1984). The specimen was tilted over approximately 70° in such a way that the incident beam direction **B** in the specimen was successively close to $[\bar{1}01]$ (fig. 20(a)), $[\bar{3}11]$ (Fig. 20(b)), $[\bar{1}\bar{1}3]$ (Fig. 20 (c)), $[\bar{1}13]$(Fig. 20(d)) and $[\bar{3}\bar{1}1]$(Fig. 20(e)). The dislocation is sketched schematically and labelled in fig. 20(f).

As can be seen from figs.20(a)-(e), all the segments studied appear as single dislocations when viewed along appropriate directions contained in the glide plane. Since superpartials can be clearly resolved for all segments as the specimen is tilted, it can be concluded that all the segments are climb dissociated. The geometry of the climb dissociation is sketched in fig. 21. The following features can be seen.

(1) Even the segments in the pure screws orientation lie off the original slide plane; they lie on a plane on which the adjacent non-screw segments are climb dissociated.
(2) Two superpartials do not cross over in the pure screw orientation, when they pass from one side of the pure screw to the other side. This can be seen from fig. 22 which is an enlarged picture of fig. 20(b).
(3) Climb dissociation takes place along two directions, namely <011> and <113>. This is always

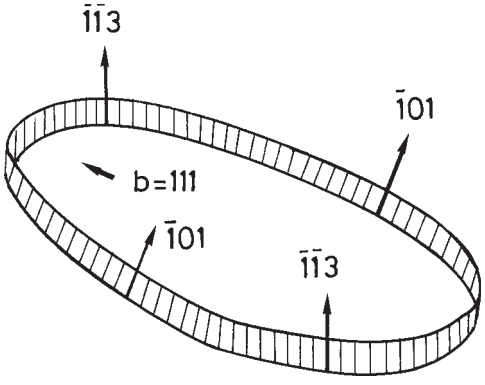

Fig. 21 A schematic illustration of the climb-dissociated [111] superlattice dislocation shown in fig. 21. All the segments are climb dissociated along two directions, namely <110> and <113>.

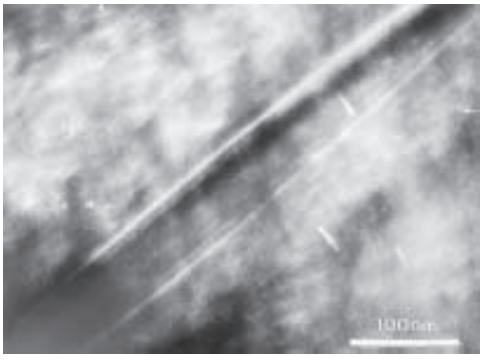

Fig. 22 An enlarged picture of fig. 20(b). The two superpartials in pure screw are parallel and do not cross over.

true, and climb dissociation along directions other than these two directions has never been observed.

Similar tilting experiments carried out on the dislocations introduced by deformation below Tp have shown that, even at room temperature or 77K, edge components are climb dissociated, although screw components lie on the original glide plane.

8. Discussion to Results described in Sections 2-7

8.1 Energy of climb-dissociated dislocations

Before discussing the mechanisms for the strength anomaly of β-brass based on the results described so far, it is necessary to confirm that the climb dissociation does not take place after the deformation by absorbing nearby vacancies during either cooling or specimen preparation. This explanation an be excluded for the following reasons. If this were true, the dislocations introduced by 77K deformation, which are kept at room temperature during specimen preparation, would be climb dissociated in the same manner as those introduced by the room-temperature deformation; this is not the case.

The energy of <111> superdislocations in the climb-dissociated configuration (E_C) and the glide-dissociated configuration (E_g) may be expressed as

$$E_C = E_1 + E_2 + E_{c12} + g_{cy}, \tag{1}$$
$$E_g = E_1 + E_2 + E_{g12} + \gamma_{gx}, \tag{2}$$

Where x and y are the separations of the two 1/2<111> superpartials in the glide-dissociated and climb-dissociated configurations, respectively, E_1 and E_2 are the self-energies of the two superpartials, γ_g and γ_c are the energies of the antiphase boundaries (APB) on the glide plane and the climb plane, respectively, and E_{g12} and E_{c12} are the interaction energies between the two superpartials in the glide-dissociated and the climb-dissociated configurations, respectively.

The self-energies E_1 and E_2 can be expressed within the framework of isotropic elasticity in the form

$$E_1 = E_2 = \mu b^2/4\pi \{\cos^2\theta + \sin^2\theta/(1-\upsilon)\}\ln R/r_o, \tag{3}$$

Where μ is the shear modulus, υ is the Poisson ratio, b is magnitude of the Burgers vector of the superpartials, R and r_o are the usual outer and inner cut-off radii, and θ is the angle between the dislocation line and the Burgers vector.

E_{c12} and E_{g12} can be written in the form (Hirth and Lothe 1968)

$$E_{c12} = (\mu\, b^2/2\pi)\{\ln(R/y) - \sin^2\theta\}, \tag{4}$$
$$E_{g12} = (\mu\, b^2/2\pi)\{\ln(R/x)\} \tag{5}$$

Thus, the difference in energy between climb dissociation and glide dissociation ΔE is given by

$$\Delta E = E_C - E_g = (\mu\, b^2/2\pi)\{\ln(x/y) - \sin^2\theta\} + \gamma_{cy} - \gamma_{gx} \tag{6}$$

Substituting the equilibrium value for x and y ($x=\mu b^2/2\pi\gamma_g$, $y=\mu b^2/2\pi\gamma_c$) into eqn.(6), We obtain the simple equation

$$\Delta E = (\mu b^2/2\pi)(- \ln\Gamma + \sin^2\theta), \tag{7}$$

Where $\Gamma = \gamma_c/\gamma_g$.

When $\Delta E < 0$, the energy of <111> superdislocations in the climb-dissociated configuration is lower than in the glide-dissociated configuration, and vice versa (see fig. 23). When Γ=1, that is when the energy of the antiphase boundary γ_{APB} is isotropic, the energy of climb dissociation is always lower than that of glide dissociation except for pure screw, for which $E_C = E_g$. On increasing Γ, the range over which limb dissociation is energetically favoured decreases from $0° < \theta < 90°$ for $\Gamma = 1$ to $25° < \theta < 90°$ for $\Gamma = 1.2$. Thus, it may be said that, except for near-screw orientations climb dissociation has a lower energy than glide dissociation when γ_{APB} is fairly isotropic.

8.2 Inverse temperature dependence of the yield stress and the transition of slip direction

The climb of 1/2<111> superpartials having an edge component proceeds by interactions with point defects. The formation energy of vacancies in β-brass is very low (0.45eV) (Koczak, Herman and Damask 1971), so that a substantial number of vacancies exist at moderate temperature. Suppose that one of the superpartials, say the leading one, climbs during the glide motion by a distance y' with respect to the trailing one (fig. 23). The energy of such a [111] superdislocation in edge orientation may be expressed as

$$E' = E'_1 + E'_2 + E'_{12} + \gamma_{111}\, y' + \gamma_{110}\, x', \tag{8}$$

where E'_1 and E'_2 are the self energies of the leading and trailing superpartials in edge orientation, γ_{111} and γ_{110} are the APB energies on the (111) and $(\bar{1}01)$ planes, respectively, and E'_{12} is the interaction energy between the two superpartials. The self-energies E'_1 and E'_2 of superpartials in edge orientation can be expressed in the form

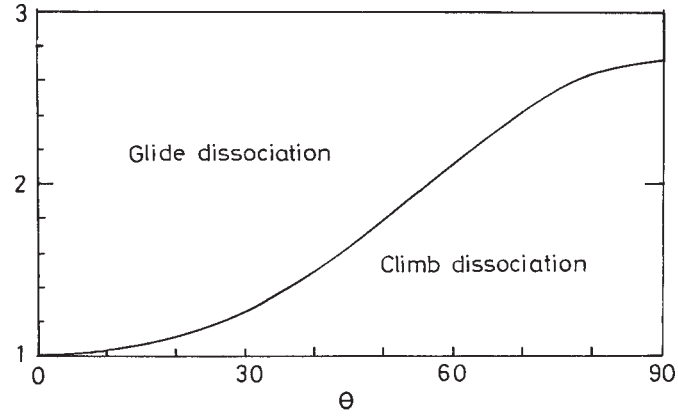

Fig. 23 The criterion for the stability of glide and climb dissociation as functions of Γ and θ, where $\Gamma = \gamma_c/\gamma_g$, and θ is the angle between the dislocation line and the Burgers vector.

$$E'_1 = E'_2 = (Kb^2/4\pi)\ln(R/r_o) \quad (9)$$

Where K is the energy factor.
The interaction energy E'_{12} is expressed for pure edge orientation in the form (Hirth and Lothe 1968)

$$E'_{12}=(Kb^2/2\pi)[\ln R/(x^2 + y^2)^{1/2} - y^2/(x^2 + y^2)]. \quad (10)$$

The energy E' and the force on the superpartials were calculated as functions of x' and y' and are shown in fig. 24. In this calculation the value cited by Potter (1969) were used for K, R and ro; for γ_{110} the experimentally determined value (Saka *et al.* 1984b) was used and γ_{111} was assumed to be 1.2 γ_{110}. There are two main features of fig. 4.

(1) The energy of a climb-dissociated <111> superdislocation in edge orientation is lower than that of glide-dissociated one when y > 25A.
(2) The force needed to push the trailing superpartial to the position x=0—that is, the force needed to transform glide-dissociated <111> superdislocations into climb-dissociated ones— decreases rapidly with increasing y; if y > 40A, the trailing superpartial is attracted to the position x=0 without encountering any energy barrier.

Thus, it may be said that once one of the two superpartials climbs by a small distance with respect to the other, the glide-dissociated <111> superdislocation can easily be transformed into the climb-dissociated one. The concentration of vacancies increases with increasing temperature. Thus, at a temperature well below Tp climb of superpartials does not take place so frequently, but on increasing the deformation temperature climb becomes more and more frequent. Since the climb-dissociated <111> superpartials are sessile except for pure screw (Flinn 1960), the yield stress will also increase, and eventually at a certain temperature Tp slips other than <111> will be activated.

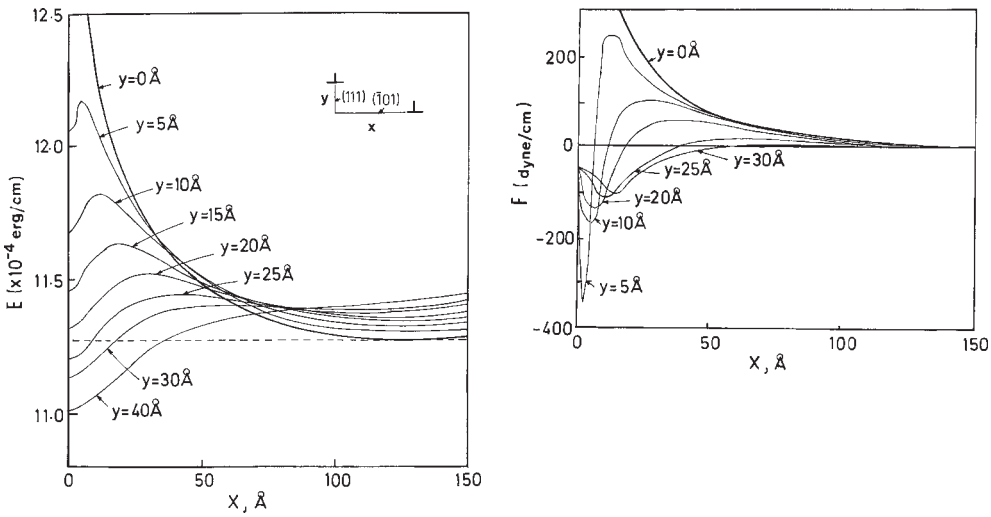

Fig. 24 The energy E' of a partially climb-dissociated [111] superdislocations in edge orientation, and the forces F' on the superpartials, as functions of x and y. γ_{110} is taken to be 50 ergcm^{-2} (Saka *et al.* 1984b) and γ_{111} is assumed to be 1.2γ_{110}.

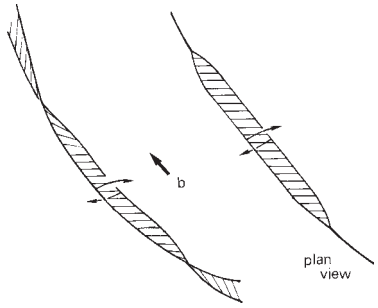

Fig. 25 Mechanism by which the pure screw [111] superlattice dislocations become dissociated off the original glide plane. The pure screw superpartials are rotated by the line tension of the adjacent non-screw dislocations which have already been climb dissociated.

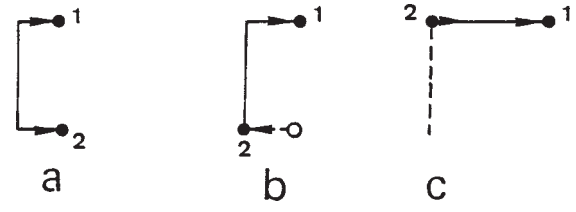

Fig. 26 Glide motion of a [111] superlattice dislocation which is dissociated off the original glide-plane. Both superpartial 1 and 2 attempt to move in the same direction under the applied stress, thereby hindering the motion of each other.

However, fig. 21 shows definitely that even the pure screw dislocations are dissociated off the original glide plane; they are dissociated on the plane on which the adjacent near-screw segments are climb dissociated. There are two possible explanations for this. One possibility is that Γ is equal to, or less than, 1. However, even when this is not the case, the line tension of those adjacent near-screw dislocations which are already climb dissociated may aid the pure screw dislocations to rotate from the original glide plane to the climb plane of these adjacent near-screw segments, as schematically shown in fig. 25.

It has been recognized that the climb-dissociated superdislocations are sessile except for pure screw dislocations (Flinn 1960). However, motion of those superdislocations in the pure screw orientation which are dissociated on a plane perpendicular to the original glide plane is also expected to be difficult. The two superpartials will attempt to glide on their original planes under the action of the applied shear stress. Therefore, before the climb-dissociated screw superdislocations can move again, one of the two superpartials must glide backwards against the applied stress and glide on a plane whose Schmid factor is very small (fig. 26). This is the situation which takes place during deformation at high temperatures, say at 463K, where even the pure screw dislocation is dissociated on that plane in which non-screw segments are climb dissociated.

On the other hand, at room temperature, where the pure screw dislocations are dissociated on the original glide plane, they can continue to glide even after the non-screw components become climb dissociated. This can explain why the yield stress at room temperature is much smaller than that at the higher temperature, despite the fact that edge dislocations are climb dissociated at both temperatures.

8.3 Pre-straining effect

8.3.1 Pre-straining at room temperature and 373K

In the case of deformation at room temperature, two facts must be taken into account. One is that edge dislocations are climb dissociated, while at least some part of screw dislocations may be dissociated on the original glide plane. The other is the so-called twinning-antitwinning polarity of plasticity (Hirsch 1968). That is, the critical resolved shear stress depends on the orientation in such a way that slip on the {211} planes in the twinning sense is easier than that in the anti-twin-

ning sense. Such a polarity is attributed to the anisotropy in the mobility of screw dislocations. Furthermore, cross-slip of screw dislocations takes place more frequently in deformation in the twinning (easy) sense than in the anti-twinning (hard) sense.

Suppose that as single crystal with the initial orientation A is pre-strained at room temperature. At this point, at least some part of the screw dislocations may be dissociated on the original glide plane (fig. 27(a)). However, the crystal is to be heated above the room temperature before the second deformation starts at high temperatures. During the heating, these screw dislocations most probably become dissociated on a plane nearly perpendicular to the original plane because of the line tension of the adjacent non-screw (edge-component-containing) segments (fig. 27(b)).

It is pointed out here that such a climb dissociation always takes place along two directions, namely along <110> and <113> (cf. fig. 21). In this sense, it can be said that the core structure of a climb dissociated dislocation has a twofold nature. For near-screw dislocations those planes which contain one of these two directions are {112} and {110}, respectively. This may be rationalized by the fact that the antiphase boundary energies on {110} and {112} planes of β-brass are very close to each other (Saka *et al.* 1984).

Suppose that a [111] $(\bar{1}01)$ superlattice screw dislocation, introduced by pre-straining at room temperature, becomes dissociated off the original $(\bar{1}01)$ plane during heating. For this dislocation, the {112}-type climb plane is determined uniquely as $(1\bar{2}1)$, because this plane is perpendicular to the original glide plane $(\bar{1}01)$. However, with regards to the {110}-type climb planes, there are two equivalent planes, namely $(0\bar{1}1)$ and $(1\bar{1}0)$. On which plane the screw dislocation becomes dissociated depends on which plane it cross-slipped on during pre-straining at room temperature.

When the dislocation is introduced by pre-straining in compression, it is most likely to have cross-slipped onto the $(\bar{2}11)$ plane, the easy-sense {211} plane for compression, while the dislocations introduced by pre-straining in tension, is most likely to have cross-slipped onto the $(\bar{1}\bar{1}2)$

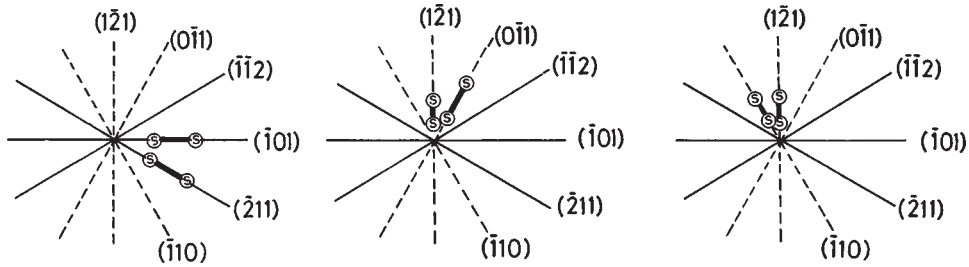

Fig. 27 (a) Configuration of superpartials in a β-brass single crystal with orientation A introduced by pre-straining in compression (twinning sense) at room temperature. Because of the polarity of the motion of screw dislocations, the screw dislocations have more probably cross-slipped onto the $(\bar{2}11)$ plane than onto the $(\bar{1}\bar{1}2)$ plane.

(b) Configuration of the superpartials, described in (a), but after being heated for the second deformation test at high temperatures. The two superpartials in pure screw orientation are now dissociated off the original glide plane by mechanism described in fig. 25. Since the dissociation of the pure screw dislocation off the glide plane always take place on both {110} and {112} planes, they are most likely dissociated on both $(1\bar{2}1)$ and $(0\bar{1}1)$ planes.

(c) Configuration of superpartials in a β-brass single crystal with orientation A pre-strained in tension (antitwinning sense) at room temperature and subsequently heated; now, they are dissociated on $(\bar{1}10)$ and $(\bar{1}21)$ planes. This configuration is equivalent to that of a β-brass crystal with orientation B which is pre-strained in compression (antitwinning sense) at room temperature and then subsequently heated.

plane, the easy-sense {211} plane for tension.

These pre-strained crystals were then deformed in either tension or compression at high temperatures. In this case, it can be assumed that only screw dislocations can move; edge dislocations are climb dissociated and completely sessile. Furthermore, the screw dislocations move on the $(\bar{2}11)$ plane whether the crystal is deformed in tension or compression because, at high temperatures, screw dislocations do not show polarity in mobility, and the glide plane is determined on the basis of the maximum resolved shear stress (fig. 28(c)). Screw dislocations which were introduced by pre-straining in compression at room temperature and then heated above room temperature are now dissociated both $(0\bar{1}1)$ and $(1\bar{2}1)$, and they must cross-slip onto the $(\bar{2}11)$ plane before they start to move. The Schmid factors for these planes are 0 and 0.25 respectively. Thus crystals pre-strained in compression at room temperature show a very high flow stress in the second deformation at high temperature, irrespective of whether they are deformed in compression or in tension in the second deformation, and the curve of flow stress against temperature for <111> screw dislocations will cross the curve of flow stress against temperature for non-<111> dislocations (fig. 28(a)) at relatively low temperatures. That is, the Tp value is low.

In contrast, when the superdislocation is introduced by pre-straining in tension at room temperature, it is most likely to have cross-slipped onto the $(\bar{1}\bar{1}2)$ plane, the easy-sense {211} plane for tension. Thus, after pre-straining and heating, it is dissociated on the $(\bar{1}10)$ and the $(1\bar{2}1)$ planes (fig. 27(c)). The Schmid factors for these planes are 0.43 and 0.25 respectively. Thus, on subsequent deformation these screw dislocations must glide on $(\bar{2}11)$ plane fairly easily. In other words, crystals pre-strained in tension at room temperature show a low yield stress in the second deformation at high temperatures and the curve of low stress against temperature for <111> superlattice dislocations (fig. 28(b)) will cross the curve of flow stress against temperature for non-<111> dislocations at relatively high temperatures (fig. 28). That is, the Tp value of crystals pre-strained in tension will be higher than the Tp values of those pre-strained in compression.

The results on crystals pre-strained at 373K can be explained in a similar manner. The only difference is that the climb dissociation has already taken place in the as-pre-strained state in this case.

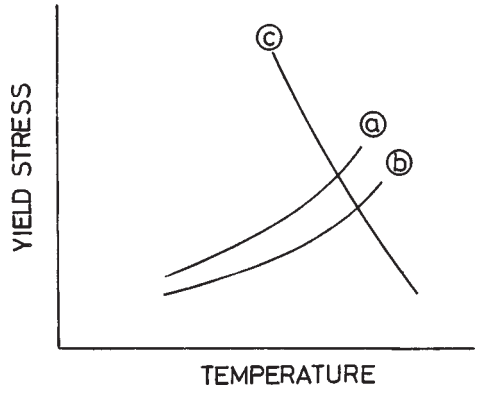

Fig. 28 Schematic diagram illustrating the occurrence of Tp in pre-strained single crystals. Curves (a) and (b) show curves of flow stress against temperature for climb-dissociated <111> dislocations introduced by pre-straining at room temperature in the twinning (easy) sense and in the antitwinning (hard) sense, respectively. Curve (c) shows flow stress for non-<111> dislocations.

Furthermore, the above discussion can be applied to pre-straining effect of crystals with the initial orientation B. In this case, tension corresponds to the easy-sense deformation, and compression to the hard-sense deformation. Thus, the Tp value of crystals pre-strained in tension is expected to be lower than the Tp value of those pre-strained in compression, and this is exactly what is observed in fig. 12(b).

8.3.2 Pre-straining at 77K

When a crystal is pre-strained at 77K, neither edge nor screw components are climb dissociated. All the segments are glide dissociated. In addition, since at 77K the mobility of edge dislocations is much larger than that of screw dislocations, those screw dislocations which are introduced by the deformation at 77K are likely to be very long and straight. During the heating of the crystal for the second deformation, the edge dislocations are climb dissociated. However, the screw dislocations, which are very long and straight, most probably remain dissociated on the original glide plane because, in this case, non-screw segments are too far away to rotate the pure screw segment from the original glide plane to the climb plane.

Suppose that such a pre-strained crystal is deformed at high temperatures in the second deformation. As discussed already, since pure screw dislocations lie on the original glide plane, they can start to glide at a stress level which is much lower than that necessary to start those screw dislocations lying perpendicular to the original glide plane. Thus, it is expected that the flow stress of crystals pre-strained at 77K is much lower than that of those pre-strained in compression at room temperature and hence the Tp value obtained in the second deformation will be higher. This is exactly what is observed in fig. 13.

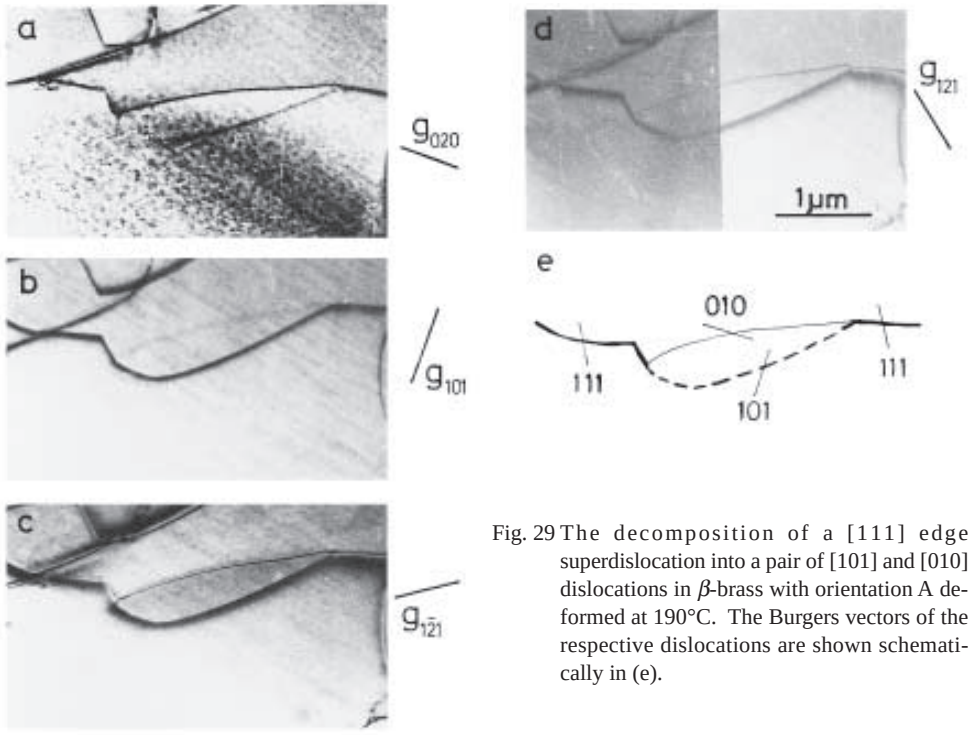

Fig. 29 The decomposition of a [111] edge superdislocation into a pair of [101] and [010] dislocations in β-brass with orientation A deformed at 190°C. The Burgers vectors of the respective dislocations are shown schematically in (e).

8.4 Formation of non-<111> dislocations

Non-<111> dislocations can be formed from single <111> superdislocations by the reactions

$$1/2[111] + 1/2\,[111] = [111], \tag{11}$$

$$[111] = [010] + [101]. \tag{12}$$

Thew former reaction, the constriction of dissociated [111] superdislocations, may take place at edge orientation where the [111] superdislocations are sessile. Once [111] undissociated dislocations are formed, they will decompose into [010] and [101] perfect superdislocations according to reaction (12) to reduce the energy, as pointed out by Bromm and Humble (1969).

Figure 29 shows direct evidence of the formation of non-<111> dislocations as a result of the decomposition of [111] superdislocations in edge orientation. The dislocations shown in fig. 29 were imaged in four different diffracting vectors, **g** = 020, 101, $1\bar{2}1$ and 121, under high-order reflection imaging conditions (Bell and Thomas 1972), where the standard **g.b** = 0 invisibility criterion is valid, even for such an elastically anistropic crystal as β-brass (Saka 1984). Figure 29(e) shows schematically the Burgers vectors of the respective dislocations. It is clear that part of a [111] superdislocation in edge orientation is dissociated into a pair of [010] and [101] dislocations.

9. Direct Pure Shear

9.1 Introduction

In the foregoing sections, it has been shown that the strength anomaly in β-brass depends not only on the orientation but also on the mode in which crystals are deformed, i.e., in tension or compression. In both tensile and compressive tests, a resolved normal stress acts on the slip plane in addition to a resolved shear stress; it is difficult to distinguish clearly between the effects of the resolved normal stress and those of the resolved shear stress. The purpose of the present section is to clarify without ambiguity whether or not Tp shows the twinning-antitwinning asymmetry, by measuring the temperature dependence of the yield stress by direct pure shear. Since it is well established that the transition of slip direction takes place at Tp from <111> direction below Tp to non-<111> direction above Tp (Saka and Kawase 1984, Saka *et al.* 1985), crystals were deformed in shear along <111> directions as well as non-<111> directions such as <100> and <110>.

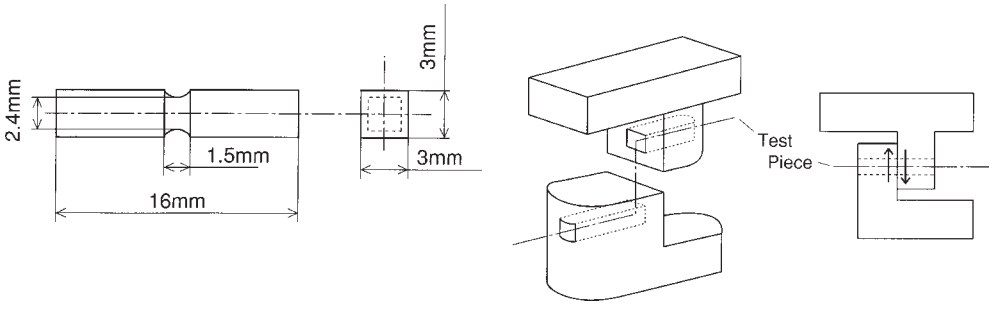

Fig. 30 (a) Shape and dimensions of the shear specimens. (b) The jig used for shear tests.

9.2 Experimental procedures

9.2.1 Shear tests

Specimens for direct shear test, of the shape and dimensions shown in fig. 30(a), were prepared by sectioning the single crystals with a multiwire abrasive saw. The cross-sectional area in the gauge length of a specimen was slightly reduced by making a groove by chemical and electropolishing.

The specimens were mounted in a special jig which allowed shear to take place over a gauge length of 1.5mm (fig. 30(b)). The deformation was carried out in an Instron-type machine at a shear strain rate of $2 \times 10^{-4} s^{-1}$ between 100 and 300°C. The shear was applied along the <111>,<100> and <110> directions and the planes of direct shear were {112} and {110} types for <111> shear, and {100} and {110} types for non-<111> shear.

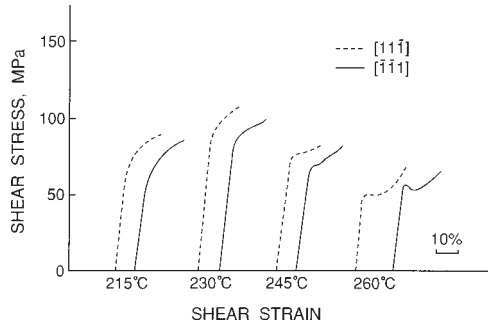

Fig. 31 Examples of shear stress-shear strain curves of crystals deformed on the (101) shear plane. The shear directions were either [$\bar{1}\bar{1}$1] or [11$\bar{1}$].

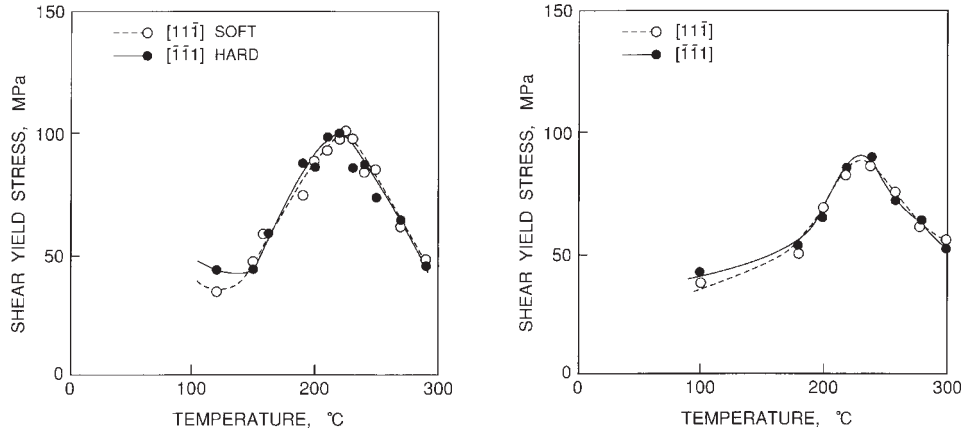

Fig. 32 (a) Temperature dependence of the shear stress: (○), yield stresses for slip on [11$\bar{1}$](101); (●), yield stresses for slip on[$\bar{1}\bar{1}$1](101).
(b) Temperature dependence of the shear stress: (○), yield stresses for slip in easy sense on [11$\bar{1}$]($\bar{2}$11); (●), yield stresses for slip in hard sense on[$\bar{1}\bar{1}$1]($\bar{2}$11).

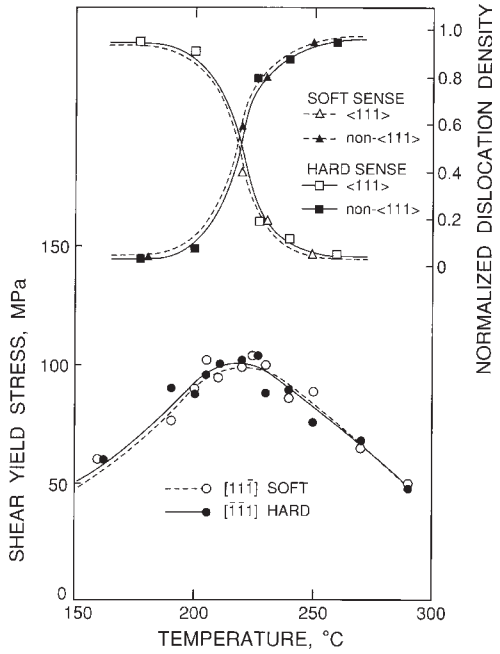

Fig. 34 Normalized densities of <111> and non-<111> dislocations plotted against the deformation temperature, together with the shear yield stress for crystals deformed in the hard (antitwinning) sense(●) and in the easy (twinning) sense (○). The normalized densities were obtained by dividing the length o the respective dislocations by the total length of dislocations studied.

9.2.2 Optical and electron microscopy

Slip lines were observed on the top-surfaces using a Normarski interference microscope, and the slip planes determined. Foil specimens were prepared and examined in a JEOL 200CX microscope and the Burgers vectors of dislocations determined.

9.3 Results

9.3.1 <111> slips

Figure 31 some typical examples of stress-strain curves obtained for crystals deformed in direct shear along [11$\bar{1}$] and [$\bar{1}\bar{1}$1] on (10$\bar{1}$) plane at different temperatures. Figure 31(a) shows the temperature dependence of the nominal yield stress of β-brass deformed in direct shear along <111> on (101) plane. Data points obtained in shear along [11$\bar{1}$] are shown by open circles and those obtained in shear along [$\bar{1}\bar{1}$1] are shown by full circles. No significant difference was observed between them.

Figure 32 shows some typical examples of stress-strain curves obtained on crystals deformed in direct shear along <111> in the twinning (easy) sense on {112} plane and in the antitwinning (hard) sense on {112} plane at different temperatures. Figure 32(b) shows the temperature dependence of the nominal yield stress of β-brass deformed in direct shear along <111> on {112} plane in the twinning (easy) and antitwinning (hard) senses. No significant difference was observed between twinning(easy) sense and antitwinning (hard) sense except at very low temperature.

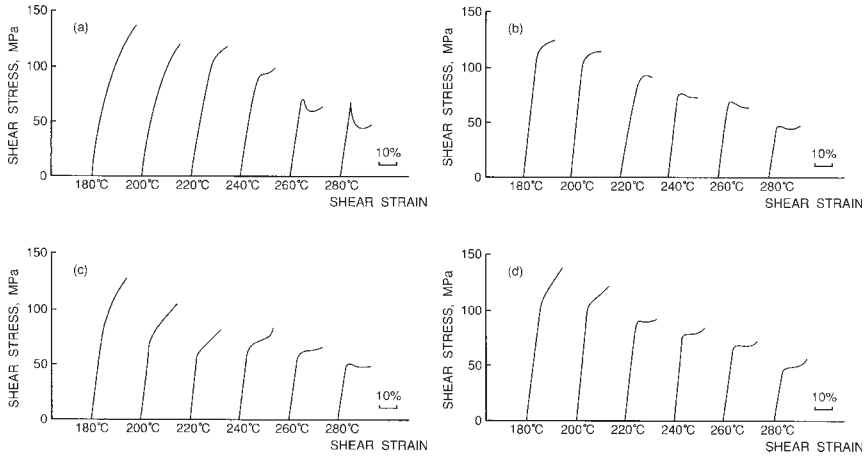

Fig. 35 Examples of shear stress-shear strain curves of crystals deformed at different temperatures for (a)[10$\bar{1}$](101), (b)[010](101), (c)[100](010) and (d)[101](010) shear systems.

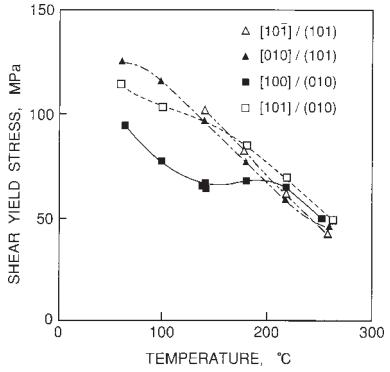

Fig. 36 Temperature dependence of the shear yield stress for the [10$\bar{1}$](101) (△), [010](101) (▲), [100](010) (■) and [101](010) (□) shear systems.

Optical microscopy of slip lines on the top faces shows that, in both {101} and {112} shears, <111> dislocations operate above Tp and non-<111> dislocations below Tp. Figure 34 shows the densities of <111>,<101> and <010> dislocations as a function of the deformation temperature. It is evident that there is a coincidence between the strength peak and the transition of slip direction, whether crystals were deformed in the easy sense or in the hard sense. From this figure it can be concluded that no asymmetry in Tp with respect to a reversal of the sign of the shear stress was observed.

9.3.2.Non-<111> shear

Figure 35 shows some examples of stress-strain curves obtained on crystals deformed in direct shear in different shear systems containing the shear direction other than <111>. Except for two stress-strain curves where crystals were deformed in shear in the [10$\bar{1}$](101) system at 180°C and 200°C and the yield stress was rather difficult to detect, the nominal yield shear stress could be determined without ambiguity as a sharp change in the slope of a stress-strain curve. Figure 36

shows the temperature dependence of the nominal yield shear stress for the four systems containing non-<111> shear directions.

It is noted that the critical shear stress in the [100](010) slip system shows a peak at around 240°C.

10. Shear Superimposed with a Normal Stress

10.1 Effect of superimposition of compressive normal stress on the yield stress of β-brass measured in direct shear

10.1.1 Experimental procedures

In order to apply a compressive stress normal to the shear plane of a specimen which was being directly sheared, special jigs were attached to an Instron-type testing machine (fig. 37(a)). A pair of arms A were attached to the outer movable shell MS, which was in turn fixed to the crosshead CH of the testing machine. The specimen, placed between these arms, was compressed when the arms A were pushed together with a motor M. In order to avoid buckling of the specimen a compressive stress was applied via spacers Sp which were placed between the arms and the specimen. Also, in order to avoid friction between these spacers and the arms, a pair of flat roller FR was placed between the arms A and the spacers Sp. The normal stress applied to a specimen was measured with a load cell LC and kept well below the yield stress, that is within the elastic region. The four shear systems [100](010), [010](101), [101](010) and $[\bar{1}01](101)$ were studied.

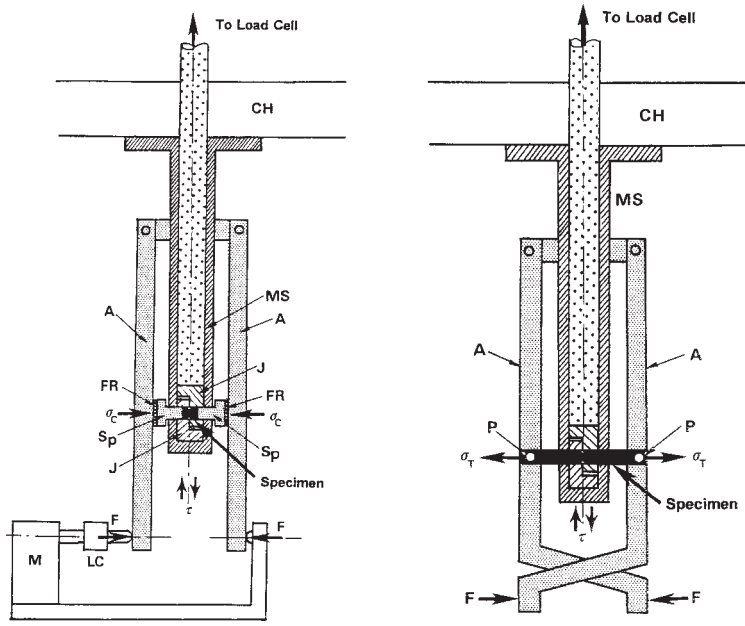

Fig. 37 Special jigs attached to an Instron-type testing machine in order to superimpose a normal compressive stress (a) and a normal tensile stress (b) to a shear plane.

10.1.2 Results

Figure 38 shows some typical examples of shear stress-shear strain curves obtained at different temperatures in the [100](010) shear tests with different levels of normal compressive stress, σ_c superimposed. In this case, virgin crystals were used to obtain each of the stress-strain curves. In the curves the shear yield stress τ_{yc} can be determined clearly, and it is clear that τ_{yc} increased with increasing σ_c.

Figure 39 shows similar shear stress-shear strain curves. In this case, however, identical crystals were used; shear tests were interrupted and the level of the compressive stress was increased or decreased in a stepwise manner. Again, it is clear that the shear stress τ_{yc} increased with increasing normal compressive stress σ_c.

10.2 Effect of superimposition of tensile normal stress on the yield stress of β-brass measured in direct shear

10.2.1 Experimental procedures

In order to apply a tensile stress normal to the shear stress of a specimen which was being directly sheared, the apparatus used to apply a normal compressive stress during a direct shear test (Matsumoto *et al.* 1995) was slightly modified, as is shown in figure 37(b). A pair of arms A were attached to the movable shell MS, which was in turn fixed to the cross-head CH. The arms A were staggered so that a specimen, placed between these arms, was stretched when the arms A were pushed together with a motor F. The specimen was connected to the arms A with a pair of pins P. The normal stress applied to a specimen was measured with a load cell (not shown) and kept at 40Mpa, well below the yield stress. The four shear systems <100>{100}, <100>{110}, <110>{100} and <110>{110} were studied.

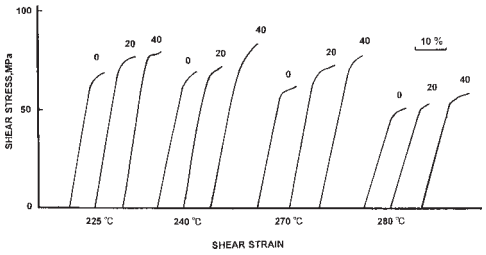

Fig. 38 Some typical examples of shear stress-shear strain curves obtained at different temperatures in the shear tests on the [100](010) shear system with different levels of compressive stress σ_c. The numbers on each of the curves refer to σ_c in MPa.

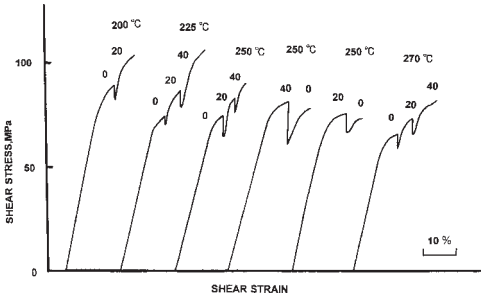

Fig. 39 Sear stress-shear strain curves similar to those shown in fig. 38. In this case, identical crystals were used; shear tests were interrupted and the level of the compressive stress σ_c superimposed on the specimen being sheared was increased or decreased in a stepwise manner. The numbers on each of the curves refers to σ_c in Mpa. The flow stress was calculated by subtracting an increment in stress owing to strain hardening.

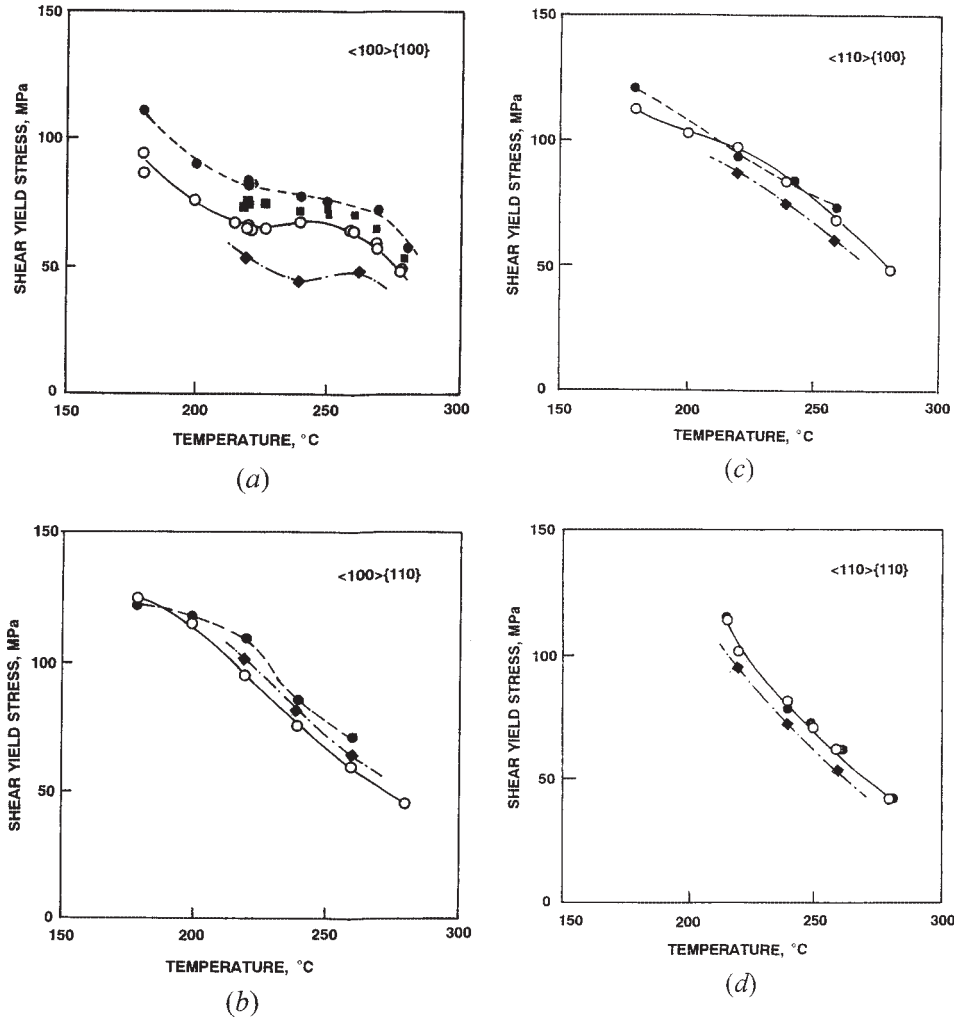

Fig. 40 Summary of the effect of a superimposed normal stress on the shear yield stress of the four different shear systems (a) <100>{100}, (b)<100><{110}, (c) <110>{100} and (d) <110>{110} studied: (○), τ_{yp} yield stress in the absence of the superimposed normal stress (Matsumoto and Saka 1993); (■),τ_{yc}, yield shear stress in the presence of a normal compressive stress of 20Mpa (Matsumoto *et al*. 1995); (●),τ_{yc}, yield shear stress in the presence of a normal compressive stress of 40Mpa (Matsumoto *et al.* 1995); (◆), τ_{yt}, yield shear stress in the presence of a normal tensile stress of 40Mpa (Matsumoto and Saka 1997).

10.2.2 Results

The yield shear stresses τ_{yt} and τ_{yc} obtained in this way for the four different shear systems are plotted against temperature, together with the yield stresses τ_{yp} obtained in pure shear tests (Matsumoto and Saka 1993) in figure 40. Except for the <100>{100} shear system, τ_{yt}, τ_{yc} and τ_p are more or less at similar levels. In contrast, in the <100>{100} shear system, a normal stress has a profound effect on the shear yield stress; τ_{yt} is substantially lower than τ_p, and τ_{yc} is substantially higher than τ_p.

11. Cyclic Deformation

11.1 Introduction

Tp depends on not only the crystal axis but also whether the crystal is deformed in tension or compression. In particular, when crystals with orientation A are deformed uniaxially, the Tp value obtained in compression, Tpc, is around 150°C, while the Tp value obtained in tension, Tpt, is around 250°C, the difference being as much as 100°C. Furthermore, the occurrence of the strength peak is always accompanied by a transition of the slip direction. Below Tp slip always takes place along <111> directions while, above Tp, it takes place along some non-<111> directions.

Therefore it would be very interesting to study which dislocation structure dominates when β-brass single crystals with orientation A are deformed cyclically in push-pull in the temperature range between Tpc and Tpt, say at 200°C.

11.2 Experimental Procedures

Single crystals with orientation A were deformed in push-pull with a self-aligning grip system. The elastic strain in hysteresis loops were electrically cancelled and only the plastic strain recorded in order for the condition of constant plastic strain amplitude to be satisfied. The deformation was made at a constant strain rate of 2×10^{-4} s^{-1} at 200°C. The strain amplitude was kept constant at $\pm 9 \times 10^{-4}$. The specimens used are shown in table 2.

11.3 Results

11.3.1 Cyclic deformation starting from tension

The dislocation structure of specimen deformed in the first half-cycle (Nc=1/2) starting from tension (specimen T), that is, the dislocation structure after a simple tensile test consists of <111> dislocations (Saka *et al.* 1985).

Table 2 Specimens used in cyclic deformation at 200°C

Crystal Number	Numbers of cycles, Nc	Deformation Start	Finish	Type of dislocations
T	1/2	Tension	Tension	<111>
C	1/2	Compression	Compression	non-<111>
F9	1	Compression	Tension	<111>
F52	1	Tension	Compression	<111>
F5	4 + 1/2	Tension	Tension	<111>
F4	5	Tension	Compression	<111>
F7	5	Compression	Tension	<111>

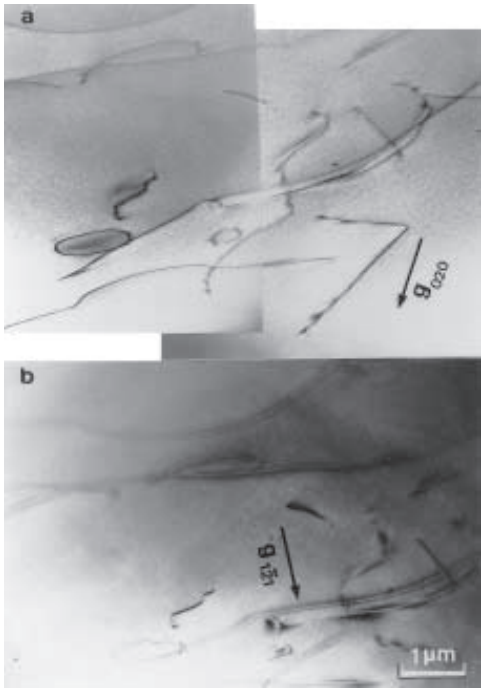

Fig. 41 Dislocation configuration in crystal F52 deformed in the first complete cycle starting from tension at 200°C. The Burgers vector of these dislocations is determined to be of <111> type.

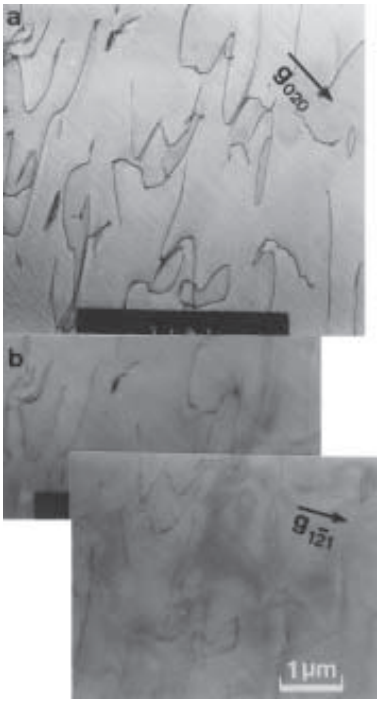

Fig. 42 Dislocation configuration in crystal F9 deformed in the first complete cycle starting from compression at 200°C. The Burgers vector of these dislocations is determined to be of <111> type.

Figure 41 shows the dislocation structures of specimen F52 deformed in the first complete cycle (Nc = 1) starting from tension. In other words, the specimen was deformed in tension, followed by deformation in compression. For **g** = $1\bar{2}1$(fig. 41(b)), almost all the dislocations show weak double images, which are characteristic for those dislocations for which **g.b** = 0. Thus, they are identified as having the Burgers vectors of <111> type. This is rather surprising in view that the dislocation after simple compression (without any pre-straining) have the Burgers vectors of no -<111> type, that is <100> and <110> (Saka and Kawase 1984).

11.3.2 Cyclic deformation starting from compression

The dislocation structure of specimen deformed in the first half-cycle (Nc = 1/2) starting from compression (specimen C), that is the dislocation structure after a simple compression consists of non-<111> dislocations, namely <101> and <010> dislocations (Saka and Kawase 1984).

Figure 42 shows the dislocation structure of specimen F9 deformed to Nc = 1 starting from compression. In other words, the specimen was deformed in compression, followed by deformation in tension. All the dislocations disappeared for g = $1\bar{2}1$ (fig. 42(b)) and they have Burgers vectors of <111> type. This indicates that those non-<111> dislocations which had been introduced by deformation in compression in the first half-cycle must have been replaced by the <111> dislocations during the subsequent half-cycle in tension.

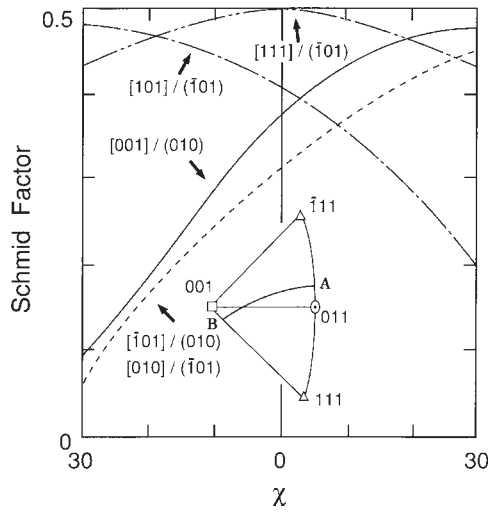

Fig. 43 χ dependence of Schmid factors for the [10$\bar{1}$](101), [010](101), [100](010), [101](010) and [111]($\bar{1}$01) slip systems. The orientation of the uniaxial loading varies along the line AB.

Thus it can be concluded that, when the crystals are deformed cyclically between Tpc and Tpt, all the dislocations activated have Burgers vectors of <111> type, except when virgin crystals are deformed in simple compression, that is in the first half-cycle starting from compression. Once the non-<111> dislocations disappear, they never appear again.

12. Discussion to Results described in Sections 9,10 and 11

A transition of slip system takes place at Tp from <111> slip below Tp to non-<111> slip above Tp (Saka and Kawase 1984, Saka *et al.* 1985). In other words, Tp can be defined as a temperature where curves of critical shear stress against temperature for <111> slip intersect with those for non-<111> slips.

For crystals with orientation B(χ = –30°), the difference between the Tp values obtained in tensile and compressive tests is rather small. On the other hand the difference is large for orientation A (χ = +30°) (Nohara *et al.* 1984, Saka and Zhu 1989). Therefore, it is reasonable to discuss the behaviour of crystals with orientations A and B.

As far as <111> slips alone are activated, applying a uniaxial stress to a crystal with χ = –30° and to that with χ = +30° is crystallographically equivalent with each other, provided that the effects of the twinning-antitwinning polarity can be neglected. However, this is no longer the case, once non-<111> slips are activated. Figure 43 shows the orientation dependence of Schmid factors of the slip systems relevant to this study. Schmid factors for [001](010), [010]($\bar{1}$01) and [$\bar{1}$01](010) slip systems are very small for crystals with χ = –30°, while for crystals with χ = +30° the Schmid factors of these slip systems are rather high. The reverse is true for [101]($\bar{1}$01) slip. Therefore it is very unlikely that the [001](010) slip is activated when a crystal with χ = –30° is deformed uniaxially.

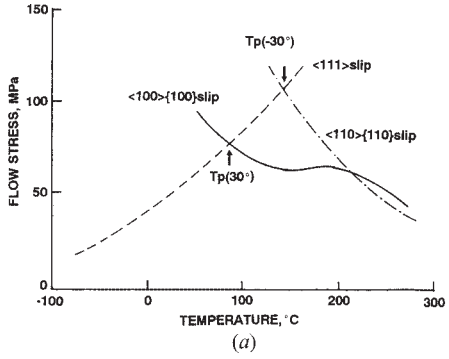

(*a*)

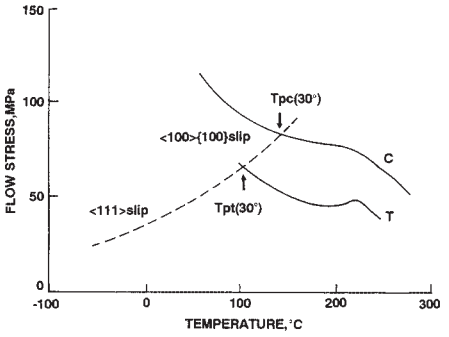

(*b*)

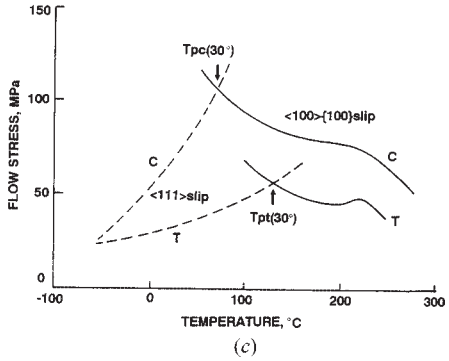

(*c*)

Fig. 44 (a) Mechanism to explain the stress anomaly in β-brass with $\chi = \pm 30°$ in the absence of a superimposed normal stress.
(b) Flow stress against temperature curves for <111> slip and those for <100>{100} slip with a normal tensile (indicated by T) or compressive (indicated by C) stress superimposed.
(c) Mechanism which must be assumed to explain the tension-compression asymmetery of Tp in β-brass in terms of the normal tensile and compressive stresses on the shear yield stress.

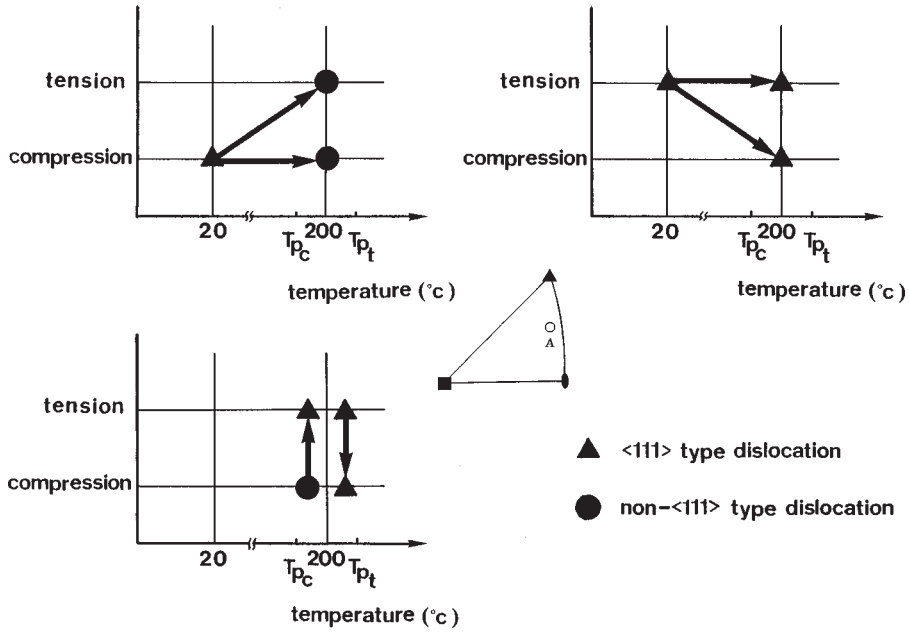

Fig. 45 Summary of transition of slip direction in β-brass with $\chi = +30°$ between T_{pc} (peak temperature obtained in compressive test) and T_{pt} (peak temperature obtained in tensile test).

Suppose that a crystal with $\chi = -30°$ is deformed uniaxially. At lower temperatures, $[111](\bar{1}\bar{1}2)$ slip should be activated while, at higher temperatures, $[101](\bar{1}01)$ slip should be activated according to a consideration based on the Schmid factors. Thus the stress peak is expected to appear at Tp(–30°), as indicated in fig. 44(a). Next, suppose that a crystal with $\chi = +30°$ is deformed uniaxially. At lower temperatures, $[111](\bar{2}11)$ slip is activated; the situation is crystallographically similar to that for a crystal with $\chi = -30°$. On the other hand, at higher temperatures, $[101](\bar{1}01)$ slip is unlikely to be activated. Among the other three non-<111> slip systems, namely [001](010), $[010](\bar{1}01)$ and $[\bar{1}01](010)$, for which the Schmid factors are rather high, [100](010) slip system is most likely to be activated at around 200°C, because the critical shear stress for this slip system is much lower than those of the others (see fig. 36). Thus the stress peak appears at Tp(–30°) as indicated in fig. 44(a). It follows that Tp (–30°) is much higher than Tp(+30°).

So far effect of a normal stress on non-<111> dislocations has not been taken into account. As can be seen from fig. 40, effect of a normal stress on [100](010), which should operate for $\chi = +30°$, can not be neglected. If this effect is taken into account, for a crystal with $\chi = +30°$, the situation should be like fig. 44(b). It is predicted that Tpc(+30°) is higher than Tpt(+30°). Needless to say this is not the case; Tpc(+30°) should be much lower than Tpt(+30°). In order for this situation to occur, we have to invoke tension-compression asymmetry of <111> slip as schematically shown in fig. 44(c). This may not appear very sophisticated, because crystals prestrained at room temperature in tension and compression show this kind of tension-compression asymmetry (cf. fig. 28).

However, even if such an asymmetry is invoked, it is rather difficult to explain transition of slip system from non-<111> type to <111> type, when a crystal with $\chi = +30°$ is deformed cyclically between Tpc(+30°) and Tpt(+30°), say at 200°C.

Figure 45 summarizes the results for transition of slip directions for a crystal with orientation A ($\chi = +30°$). Excepting the behaviour of a crystal with orientation A between Tpc(+30°) and Tpt(+30°), strength anomaly in β-brass can be explained by climb dissociation of <111> dislocations between room temperature and Tp and transition of the slip direction from <111> below Tp to non-<111> above Tp.

Acknowledgements

Many students have been involved in this study. Especially, contributions by Mr. M. Kawase, Dr. Yumei Zhu and Dr. A. Matsumoto are acknowledged. The author thanks Dr. A. Nohara for stimulating discussion during this study.

References

Ardley, G. W., and Cottrell, A. H., 1953, Proc. R. Soc. A, **219**, 328.

Bell, W. L., and Thomas, G., 1972, *Electron Microscopy and Strength of Materials*, edited by G. Thomas, R. M. Fulrath and R. M. Fisher (Berkley, Los Angeles: University of California Press), p.23.

Broom, N., and Humble, P., 1969, Phil. Mag., **19**, 639.

Cockayne, D. J. H., Ray, I. L. F., and Whelan, M. J., 1969, Phil.Mag., **20**, 1265.

Koczak, M. J., Herman, H., and Damask, A. C., 1971, Acta metall., **19**, 303.

Flinn, P. A., 1960, Trans. Am. Inst. Min. Metall. Engrs, **218**, 145.

Head, A. K., 1967, Phy. Stat. sol., **19**, 185.

Hirsch, P. B., 1968, Trans. Japan Inst. Metals, **9** (Suppl.), xxx.

Hirsch, P. B., Howie, A., Nicholson, R. B., Pashley, D. E., and Whelan, M. J., 1965, *Electron Microscopy of Thin Crystals* (Butterworth).
Hirth, J. P., and Lothe, J, 1968, *Theory of Dislocations* (New York: McGraw-Hill).
Matsumoto, A., Mizoguchi, K., and Saka, H., 1995, Phil. Mag., A., **72**, 1189
Matsumoto, A., and Saka, H., 1993, Phil. Mag., A, **67**, 217.
Matsumoto, A., and Saka, H., 1997, Phil. Mag. Lett., 76, 391.
Nohara, A., Izumi, M., Saka, H., and Imura, T., 1984, Phys. Stat. Sol. (a), **37**, 719. 1984
Potter, D. I., 1969, Materi. Sci. & Engg, **5**, 201.
Saka, H., 1984, Phil. Mag. A, 49, 327.
Saka, H., and Kawase, M., 1984, Phil. Mag., A, **49**, 525.
Saka, H., Kawase, M., Nohara, A., and Imura, T., 1984, Phil. Mag., A, **50**, 65.
Saka, H., and Zhu, Y. M., 1985, Phil. Mag. A, **51**, 629.
Saka, H., and Zhu, Y. M., 1989, Materi. Sci. & Engg., A**113**, 305.
Saka, H., and Zhu, Y., 1994, Phil. Mag., A., **69**, 1155.
Saka, H.,Zhu, Y. M., Kawse, M., Nohara, A., and Imura, T., 1985, Phil. Mag., A, **51**, 365.
Umakoshi, Y., Yamaguchi, M., Namba, Y., and Murakami, Y., 1976, Acta metall., **24**, 89.
Zhu, Y. M., and Saka, H., 1986, Phil. Mag., A., **54**, 783.
Zhu, Y. M., and Saka, H., 1989, Phil. Mag., A., **59**,6 61.

DOCTORAL DISSERTATIONS

(1999.4.1 – 2000.3.31)

Applied Chemistory

Name	Title	Diss. No.	Date
Uno, Takahiro	Stereospecific polymerization of α-substituted acrylates	K1365	1999.10.29
Inagaki, Kazumi	Multielement correlation analysis and chemical speciation of trace elements in human blood serum as studies by analytical atomic spectrometry	K1376	1999.3.27
Ji, Shan	Multielement profiling analyses of the elemental distributions between seawater and natural salt as studied by analytical plasma spectrometry (in Japanese)	K1377	1999.3.27
Kojima, Takashi	Study on creation of Zirconia-based composite with fracture sensing capability (in Japanese)	K1378	1999.3.27
Shimizu, Ken-ichi	Molecular bases for the design of metal oxide De-Nox catalysts	K1379	1999.3.27
Suzuki, Kazuyuki	Synthesis and evaluation of ferroelectric K(Ta,Nb)O3 thin film (in Japanese)	K1380	1999.3.27
Ishida, Yasuyuki	Characterization of polymeric materials and natural organic compounds by reactive pyrolysis-gas chromatography (in Japanese)	R1420	1999.4.30
Takaku, Yuichi	Development of high-sensitive analytical methods for environmental and biological samples by inductively coupled plasma mass spectromerty	R1426	1999.6.30
Sakai, Takenobu	Study on improvement in durability of piezoelectric ceramics (in Japanese)	R1430	1999.7.30

Applied Chemistry II

Name	Title	Diss. No.	Date
Yamazaki, Shinichi	Effects of steric hindrance and charge on local dynamics of polymer chains (in Japanese)	K1366	1999.10.29

Chemical Engineering

Name	Title	Diss. No.	Date
Yamamoto, Tsuyoshi	Analysis of combustion process in advanced energy conversion systems (in Japanese)	K1361	1999.9.30
Quitain, Armando	Reactive distillation for ethyl tert-butyl ether synthesis from bioethanol and tert-butyl alcohol	K1381	1999.3.27
Jin, Gong	Effective use of third phase in phase transfer catalytic system	K1382	1999.3.27
Tatemoto, Yuji	Biological and thermal problems for treatment of municipal solid waste (in Japanese)	K1383	1999.3.27
Tani, Koji	Study of separation and removal of trace components dissolved in water (in Japanese)	K1384	1999.3.27
Piao, Gulim	A study on combustion test of refuse derived fuel in fluidized bed (in Japanese)	K1385	1999.3.27
Kondoh, Motohiro	Properties of energy recycle by combustion of waste (in Japanese)	K1443	1999.3.27
Yamada, Hiroshi	Development of gas-liquid-liquid-solid four-phase reactor	R1452	1999.1.31

Biotechnology

Name	Title	Diss. No.	Date
Saito, Ikuo	A study of valuable microorganism in culture engineering with the aim of industrialization (in Japanese)	K1386	1999.3.27
Nakamura, Shingo	Proton-induced enantioselective reactions using chiral LBA reagents	K1387	1999.3.27
Murai, Kiyohito	A study on denitrification process by genetic engineering or improvement of wastewater treatment	K1388	1999.3.27
Moon, Kwanhoon	Development of culture system suitable for micropropagation of rice via somatic embryogenesis	K1389	1999.3.27
Yamada, Keisuke	A tissue engineering approach for construction of hybrid-type artificial liver	K1390	1999.3.27

Name	Title	Diss. No.	Date
Yamamoto, Shin	A study on bacterial glycoengineering : application for novel drug discovery	K1391	1999.3.27
Watanabe, Tsuyoshi	Catalytic enantioselective protonation of enolates using chiral proton donors	K1392	1999.3.27
Noguchi, Hideki	Analysis of biological and KANSEI information based on knowledge information processing (in Japanese)	K1444	1999.3.27
Araki, Yoshitaka	Development of asymmetric reactions directed for the preparation of enantiopure pharmaceuticals	R1427	1999.6.30
Kuribayashi, Takeshi	Aryl C-Glycosides as sialyl lewis X mimetics	R1428	1999.6.30

Materials Science and Engineering

Name	Title	Diss. No.	Date
Yamamoto, Hiroaki	Formation of hydrogen absorption alloy film by molten salts electrolysis (in Japanese)	K1445	1999.3.27
Matsumoto, Yoshihisa	Study on deformation and fracture behavior and electronic state of solute atoms in chromium (in Japanese)	R1424	1999.5.31
Kakehi, Koji	Study on high-temperature strength of single-Crystal Nickel-based superalloys (in Japanese)	R1449	1999.12.28
Nonogaki, Youichi	Study on InGaAs dots grown on InP substrate by droplet heteroepitaxy (in Japanese)	R1453	1999.1.31
Kawai, Hisataka	Study on the material properties after long-term heating and improvement in material strength of gas turbine superalloys (in Japanese)	R1458	2000.2.29
Takatsuji, Hiroshi	Reliability improvement of interconnect materials for TFT-LCD and their deposition processes (in Japanese)	R1459	2000.2.29

Materials Processing Engineering

Name	Title	Diss. No.	Date
Chino, Yasumasa	Study on control of free surface shape on a liquid metal using intermittent alternating magnetic field (in Japanese)	K1368	1999.11.30
Wang, Zhe	Predictions of microstructure and mechanical property in hot forging of vanadium microalloyed steels (in Japanese)	K1393	1999.3.27
Peiqi, Qiu	Study on semi-solid processing for cast iron (in Japanese)	K1394	1999.3.27
Sanga, Manabu	Study on influence of chemical composition and deformation condition on deformation-induced martensitic transformation in austenitic stainless steel (in Japanese)	K1395	1999.3.27
Shi, Wen	Interfacial behavior between molten magnesium and solid substrates and its application on the fabrication of magnesium matrix composites (in Japanese)	K1396	1999.3.27
Zhou, Yueming	Study on Utilization of electromagnetic force in a continuous casting of steel (in Japanese)	K1397	1999.3.27
Tajima, Nobuhiro	Preparation of hard amorphous carbon and amorphous carbon nitride thin films by shielded arc ion plating, and their structural and mechanical properties (in Japanese)	K1398	1999.3.27
Hatanaka, Shinichi	Fundamental study on design of ultrasonic fields in liquid in materials processing (in Japanese)	K1454	1999.3.27
Sonoda, Tsutomu	On surface treatment of functional Titanium-base alloy by coating technique using sputtering for improving its biocompatibility (in Japanese)	R1439	1999.10.29
Inoue, Yasushi	Study on spectroscopic process monitoring in ow-temperature plasma CVD of silicon dioxide films (in Japanese)	R1457	2000.2.29

Applied Physics

Name	Title	Diss. No.	Date
Yamane, Tsuneyuki	Measurement of thermal diffusivities of advanced materials (in Japanese)	R1431	1999.7.30
Kubota, Yoshiki	Accurate charge density analyses of laves phase intermetallic compounds (in Japanese)	R1434	1999.9.30

Nuclear Engineering

Name	Title	Diss. No.	Date
Kashibe, Shinji	Fission gas release and bubble swelling of light water reactor fuels	R1425	1999.5.31
Ito, Takahiro	Study on thermal hydraulic phenomena in advanced light water reactors with passive safety features (in Japanese)	K1370	1999.12.28
Igarashi, Hiroo	Study on water chemistry control for dose reduction based on anomalous diagnosis using BWR water chemistry data (in Japanese)	K1371	1999.12.28
Sugiyama, Takahiko	Separative analyses of packed water distillation column for hydrogen isotope separation (in Japanese)	K1399	1999.3.27
Yamakawa, Hiroshi	Separative characteristics of polyatomic gas mixture by thermal diffusion column for isotope separation (in Japanese)	K1400	1999.3.27

Electrical Engineering

Name	Title	Diss. No.	Date
Itabashi, Kaiji	A study on development of assembly motion controller including contact phenomenon (in Japanese)	K1401	1999.3.27
Kokura, Hikaru	Studies on thin films processing in high-density microwave plasmas (in Japanese)	K1402	1999.3.27
Zanma, Tadanao	Study on design method of assembly/ disassembly task system based on discret event system theory (in Japanese)	K1403	1999.3.27

Name	Title	Diss. No.	Date
Takeuchi, Ichiro	A study on fuzzy modeling of nonlinear dynamic systems (in Japanese)	K1446	1999.3.27
Chigusa, Shunji	Investigation on systematization of insulation performance of cryogenic liquids under quench conditions of superconducting power apparatus (in Japanese)	K1447	1999.3.27
Shen, Li Ping	Thesis on the stress-impedance effect in amorphous magnetostrictive wires and sensitive stress sensors using CMOS IC circuit (in Japanese)	K1448	1999.3.27
Yamano, Yasushi	Investigation on charging and discharging phenomena on dielectric surface in vacuum (in Japanese)	K1449	1999.3.27
Yubai, Kazuhiro	Study on identification and motion control of mechanical system with uncertainty (in Japanese)	K1450	1999.3.27
Inaba , Akio	Planning and control of assembly processes based on discrete event models (in Japanese)	R1421	1999.4.30
Matsushima, Isao	Laser-plasma interaction research and laser-irradiation uniformity improvement technique development for short-wavelength laser nuclear fusion (in Japanese)	R1443	1999.11.30
Iwata, Mikimasa	Study on decrease of electrode erosion in AC plasma torch and stabilization of AC arc plasma (in Japanese)	R1460	2000.2.29
Miyazaki, Akinobu	Development of long-distance gas insulated transmission line (GIL) and study of on-site testing and monitoring techniques (in Japanese)	R1461	2000.2.29

Electronics

Name	Title	Diss. No.	Date
Kawaguchi, Yasutoshi	Crystal growth of nitride semiconductors by metalorganic vapor phase epitaxy (in Japanese)	K1404	1999.3.27
Yamamoto, Kazuo	Development and applications of highly precise phase measurement technique by electron holography (in Japanese)	K1405	1999.3.27

Name	Title	Diss. No.	Date
Hayakawa, Shoji	Studies of advances in speaker recognition technology (in Japanese)	K1457	1999.3.27
Sugiura, Touko	Raman scattering study of compositional fluctuation in InGaAsP quaternary alloys (in Japanese)	R1422	1999.4.30

Information Electronics

Name	Title	Diss. No.	Date
Takeo, Kohji	Study on cell configurations for CDMA cellular systems considering non-uniformity (in Japanese)	K1372	1999.12.28
Hattori, Yoichiro	A study on construction of systems integrating patterns and symbols (in Japanese)	K1406	1999.3.27
Saruwatari, Hiroshi	A study on nonlinear array signal processing for acoustic signals	K1451	1999.3.27
Mori, Kazuo	A study on CDMA packet communications on cellular mobile communication systems (in Japanese)	K1453	1999.3.27
Kurono, Masahiro	A study of communication systems by the optical fibers laid on electric power networks (in Japanese)	R1435	1999.9.30

Information Engineering

Name	Title	Diss. No.	Date
Song, Chae-uk	Image recognition and its application to computer-aided diagnosis system of chest X-ray images (in Japanese)	K1350	1999.4.30
Hirano, Yasushi	Feature extraction of three dimensional gray images and its application to computer aided diagnosis using chest X-ray CT images (in Japanese)	K1369	1999.11.30
Fukuyasu, Naoki	CASE tool platform based on a fine grained repository and its application to software reuse (in Japanese)	K1452	1999.3.27

Name	Title	Diss. No.	Date
Ueyama, Eizo	Figure-ground separation for time-varying images by reaction diffusion advection models (in Japanese)	K1458	1999.3.27
Takada, Osamu	Methodology of building practical knowledge-based systems for design and manufacturing of products (in Japanese)	K1459	1999.3.27

Mechanical Engineering

Name	Title	Diss. No.	Date
Kinoshita, Katsuhiko	Study on effects of design parameters on air-water two-phase flow performance of a radial-flow pump for offshore oil field (in Japanese)	K1353	1999.4.30
Mizuno, Koji	The current situation of vehicle crash compatibility in Japan and its improvement	K1362	1999.9.30
Hayashi, Toshiyuki	Preparation of hard nitride thin films by ion-beam-assisted deposition and their mechanical properties (in Japanese)	K1364	1999.9.30
Ahmad, Syuhada	Heat (mass) transfer characteristics in rectangular serpentine channels with a sharp turn	K1407	1999.3.27
Kimachi, Hirohisa	Meso-mechanical study on interlaminar crack in fiber-reinforced laminated composites (in Japanese)	K1408	1999.3.27
Tanaka, Hiroshi	Fracture mechanics study on propagation of interlaminar and intralaminar cracks in carbon fiber-reinforced plastics (in Japanese)	R1432	1999.7.30
Sato, Yutaka	Effects of a new truing and dressing method on grinding characteristics of superabrasive grinding wheels (in Japanese)	R1436	1999.9.30
Shigematsu, Ichinori	Study of removal processing and surface modification with laser beam (in Japanese)	R1437	1999.9.30
Saito, Toshiyuki	Investigation of tribochemical reaction in aqueous solutions (in Japanese)	R1444	1999.11.30
Matsui, Shinsuke	Micro-Machining for optical communication devices (in Japanese)	R1445	1999.11.30

Name	Title	Diss. No.	Date
Kamiya, Soji	Development of the new copper alloy bearings for diesel engines to achieve longer life under higher load (in Japanese)	R1450	1999.12.28
Ogawa, Kazuyoshi	Study on the improvement of tooth-root fatigue strength of carburized gears (in Japanese)	R1454	1999.1.31
Shimizu, Kenichi	Fracture mechanics study on fatigue crack propagation in SiC particulate reinforced aluminum alloys (in Japanese)	R1455	1999.1.31

Mechano-Informatics and systems

Name	Title	Diss. No.	Date
Nakamura, Yuji	Numerical study of gravity effects on gas-phase spontaneous ignition over thermally irradiated solid fuel (in Japanese)	K1375	1999.2.29
Kubo, Takashi	A study on turbulent diffusion in liquid with chemical reaction (in Japanese)	K1409	1999.3.27
Ono, Koshiro	Elucidation of neck injury mechanisms during low speed rear impacts (in Japanese)	R1462	2000.2.29

Electronic-Mechanical Engineering

Name	Title	Diss. No.	Date
Odashima, Tadashi	Autonomous decentralized system design for gait pattern generation of multileged system (in Japanese)	K1410	1999.3.27
Mori, Hideo	A study on REMPI as a measurement technique for highly rarefied gas flows (in Japanese)	K1411	1999.3.27
Matsui, Hirokazu	A study on model driven shape reconstruction by matching synthesized images with actual images (in Japanese)	K1460	1999.3.27
Kato, Mitsuhiro	A study on combination tones in nonlinear continuous systems (in Japanese)	R1440	1999.10.29

Aerospace Engineering

Name	Title	Diss. No.	Date
Tanahashi, Yoshiharu	Study on aerodynamic interactions around high speed planes (in Japanese)	K1354	1999.7.30
Suzuki, Tatsuo	Control of periodic discrete-time systems (in Japanese)	R1429	1999.6.30
Kataoka, Takuya	Research on simulation of vehicle aerodynamics and thermal environment in an automobile passenger compartment (in Japanese)	R1446	1999.11.30
Hodaka, Ichijyo	Control system design based on the theory of dissipative systems (in Japanese)	R1447	1999.11.30

Civil Engineering

Name	Title	Diss. No.	Date
Sunuwar, Laxman	Evaluation of lifecycle global environmental impact of transportation infrastructures	K1355	1999.9.21
Cao, Qiuliang	Fatigue evaluation for highway bridge components under variable amplitude loading	K1356	1999.9.21
Liu, Qing Yun	Inelastic seismic design verification of thin-walled steel bridge piers	K1357	1999.9.21
Murakami, Noritaka	Study on beach deformation due to coastal structures (in Japanese)	K1367	1999.10.29
Sanada, Takeshi	Study on second order analytical solution of nonlinear diffracted waves due to offshore structures and its applications (in Japanese)	K1373	1999.12.28
Anwar, Faisal	An investigation of non-aqueous phase liquid volatilization in porous media	K1412	1999.3.27
Takaine, Toshihiro	Progressive failure in heavily/lightly overconsolidated ground by soil-water coupled finite deformation analysis and its applications to engineering problems (in Japanese)	R1433	1999.7.30
Kainuma, Shigenobu	Fatigue life evaluation and retrofitting measures for fillet welded cruciform joints in welded structures (in Japanese)	R1438	1999.9.30

Name	Title	Diss. No.	Date
Ishikawa, Yasuaki	Development of constitutive law for transient concrete as non-saturated porous material and its application to structural concrete (in Japanese)	R1441	1999.10.29

Architecture

Name	Title	Diss. No.	Date
Watanabe, Hinako	A study on arrangement of regional infrastructure for performing arts (in Japanese)	K1352	1999.4.30
Wang, Yinghua	Study on segregation in flowing process of matrix mortar in fresh concrete (in Japanese)	K1358	1999.9.30
Xu, Guohai	A study on physiological and psychological responses to fluctuating air movement (in Japanese)	K1359	1999.9.30
El-Shazly, Ali Essam	Colonial district of port city in the east and its conservation policy : comparative analysis of the European quarter in Alexandria, Egypt and the Waitan district in Shanghai, China	K1413	1999.3.27
Jin, De Yin	Nonlinear wave force effects on dynamic responses of ocean structures (in Japanese)	K1414	1999.3.27
Li, Zhuguo	Study on mechanical model of fresh mortar based on particle assembly theory (in Japanese)	K1415	1999.3.27
Kato, Kenji	The analysis of wave-induced dynamics of floating offshore structures by hybrid integral-equation method (in Japanese)	R1442	1999.10.29
Terano, Masaaki	Experimental study on thermal comfort when legs are heated in cool on slightly cool conditions (in Japanese)	R1456	1999.1.31

Crystalline Materials Science

Name	Title	Diss. No.	Date
Ishikawa, Dai	A study on the atomic arrangements and the binding energies of binary noble metal adsorbates on the Si(111) surface by means of the ion beam analysis techniques (in Japanese)	K1416	1999.3.27

Name	Title	Diss. No.	Date
Ohmori, Kenji	Study on formation and degradation of ultra-thin SiO_2 films using scanning tunneling microscopy (in Japanese)	K1417	1999.3.27
Nakatsuka, Osamu	Studies on solid-phase reactions and electrical properties at the interfaces of metals and goup-IV semiconductors (in Japanese)	K1418	1999.3.27
Liu, Xiaojun	Spectroscopic study on phase transitions in mixed-valence gold complexes	K1419	1999.3.27

Geotechnical and Environmental Engineering

Name	Title	Diss. No.	Date
Seo, Yong-Seok	Damage process in granite : experimental observation, molecular dynamics simulation and its homogenization analysis	K1360	1999.9.30
Sumi, Tetsuya	A study on heterogeneous flow in hillslope surface soil (in Japanese)	K1455	1999.3.27

Energy Engineering and Science

Name	Title	Diss. No.	Date
Ido, Takeshi	Observation of dinamic behaviors of space potential at L/H transition by a heavy in beam probe (in Japanese)	K1374	1999.2.29
Namba, Shinichi	Study on a production of a stationary high-density plasma and a population inversion in TPD-II device	K1420	1999.3.27
Kobayashi, Masahiro	Basic study on the interaction of the externally applied helical field with tokamak plasma (in Japanese)	K1421	1999.3.27
Nishimura, Akira	Studies on gas-solid fluidized bed with pulse flow operation (in Japanese)	K1422	1999.3.27
Fujisawa, Ryo	Studies on cold heat energy generation from l ow level heat energy (in Japanese)	K1423	1999.3.27

Quantum Engineering

Name	Title	Diss. No.	Date
Otsuka, Jun	Study on microwave properties of Bi-Sr-Ca-Cu-O films fabricated by multitarget sputtering (in Japanese)	K1424	1999.3.27
Ohno, Yutaka	Studies on resonant tunneling logic gates and resonant tunneling structures (in Japanese)	K1425	1999.3.27
Goto, Ryosuke	Studies on coherence control of semiconductor laser diodes by injection locking using four-wave mixing	K1426	1999.3.27
Sasajima, Naohiko	Radiation effect on Al_2O_3, $MgAl_2O_4$ and yttria-stabilized ZrO_2 under H^{2+}, He^{+} and Xe^{2+} ion irradiation	K1427	1999.3.27
Shoji, Yoshiyuki	Vaporization study on the binary rare earth alloys and rare earth-uranium alloys by mass-spectrometry	K1428	1999.3.27
Tsukimoto, Susumu	A study by in-situ TEM heating experiment on the structure and dynamical behavior of surface and interface at high temperatures (in Japanese)	K1429	1999.3.27
Furuta, Futoshi	Study of high-speed logic circuit based on Josephson Junction (in Japanese)	K1430	1999.3.27
Matsuki, Hirohisa	An investigation on fracture of a Pb-Sn solder joint on Ni-base plating (in Japanese)	K1431	1999.3.27
Moon, Won-Jin	Transmission electron microscopy study on mechanisms of deformation and fracture in ceramics	K1432	1999.3.27
Sasaki, Yukichi	Microstructure analysis of zeolites by low dose observation using transmission electron microscopy (in Japanese)	K1456	1999.3.27
Nakahara, Hitoshi	Studies on molecular beam epitaxial growth control and surface reconstruction (in Japanese)	R1463	2000.2.29

Micro System Engineering

Name	Title	Diss. No.	Date
Itoh, Tomotaka	A study on new design method of practical teleoperation system for human-machine collaboration : task-oriented control of telemanipulator based on passivity (in Japanese)	R1423	1999.4.30
Kobayashi, Futoshi	A study on sensor fusion system (in Japanese)	K1351	1999.4.30
Uematsu, Kenji	Bracing control of redundant manipulator (in Japanese)	K1433	1999.3.27
Tanimoto, Mitsutaka	A study on a tale-medicine system for intravascular neurosurgery (in Japanese)	K1434	1999.3.27
Nakanishi, Jun	A Brachiating robot controller	K1435	1999.3.27
Higashi, Toshimitsu	Self-organizing AGV transportation system adapting to dynamical environment (in Japanese)	K1436	1999.3.27
Yoshioka, Tetsuo	On-chip tensile testing of micromaterials (in Japanese)	K1437	1999.3.27
Yoneda, Mitsunori	A study on performance improvement of crane system with interactive adaptation interface (in Japanese)	K1438	1999.3.27
Isogai, Masahiro	Study on intelligent fault diagnosis for vibration control system of flexible structures (in Japanese)	K1461	1999.3.27
Ohshima, Yasuji	A study on measurements of micro-tribological phenomena in head-disk interface (in Japanese)	K1462	1999.3.27
Yamaji, Kouki	Mechatronics design and practical education : from view point of robot control and energy converter (in Japanese)	R1448	1999.11.30

Molecular Design and Engineering

Name	Title	Diss. No.	Date
Yoshida, Yoshifumi	Compression behavior of fine particle network structure in liquid (in Japanese)	K1439	1999.3.27
Akasaka, Tsukasa	Syntheses, characterizations, and functions of DNA-carbohydrate conjugates	K1440	1999.3.27

Name	Title	Diss. No.	Date
Kojima, Yoshihiyo	Quantification of ultrasonic intensity by chemical dosimetry and its application to polymerization of styrene (in Japanese)	K1441	1999.3.27
Yashiro, Arihiro	Molecular design of [60] fullerene glycoconjugates via [3+2] cycloaddition	K1442	1999.3.27

Computational Science and Engineering

Name	Title	Diss. No.	Date
Kondo, Toshiyuki	A study on evolutionary construction of adaptation mechanism for autonomous mobile robots	K1363	1999.9.30
Yamamoto, Satoru	Study of development and application of a new simulation method for fiber and platelike particle dispersed systems (in Japanese)	R1451	1999.12.28